Synthesis and Characterization of MgAlON-BN Refractories

ZUOTAI ZHANG

KTH Industrial Engineering
and Management

Doctoral Thesis

Stockholm, Sweden 2006

ROYAL INSTITUTE
OF TECHNOLOGY

Synthesis and Characterization of MgAlON-BN Refractories

Zuotai Zhang

Doctoral Thesis

Department of Materials Science and Engineering

Royal Institute of Technology

Stockholm, Sweden

2006

Akademisk avhandling som med tillstånd av Kungliga Tekniska Högskolan i Stockholm, framlägges för offentlig granskning för avläggande av Teknologie doktorsexamen, fredagen den 31 Mars 2006, kl. 10.00 i Salongen, KTHB, Osquars Backe 31, KTH, Stockholm.

ISRN KTH/MSE--06/01--SE+THMETU/AVH

ISBN 91-7178-271-0

Zuotai Zhang *Synthesis and Characterization of MgAlON-BN Refractories*

KTH School of Industrial Engineering and Management
Department of Materials Science and Engineering
Royal Institute of Technology
SE 100 44 Stockholm
Sweden

ISRN KTH/MSE--06/01--SE+THMETU/AVH
ISBN 91-7178-271-0

Abstract

In order to meet the need of metallurgical industry in the world, a new MgAlON-BN composite which can be used for example in special refractory nozzles, tubes and break rings for the continuous casting of steel was studied in the present thesis. The aim was to understand the mechanism of synthesis and their physicochemical properties during the application. Thus, the thermodynamic properties, synthesis process, mechanical properties, thermal shock behaviour, thermal diffusivity/conductivity as well as corrosion resistance to molten iron containing oxygen and molten slag of MgAlON and MgAlON-BN composites have been investigated.

The Gibbs energy of formation of MgAlON was estimated using the method proposed by Kaufman. The phase stability diagram of Mg-Al-O-N-B was investigated, and consequently the synthesis parameters were determined. MgAlON and MgAlON-BN composites were fabricated by hot-pressing method. The composites obtained this way were characterized by XRD, SEM, TEM and HREM analyses. A Matrix-flushing method was employed in the quantitative XRD analysis for the multi-component samples to understand the mechanism of synthesis.

The relationship between mechanical properties and microstructure of the composites was investigated. The experimental results indicated that BN addition has significant influence on the mechanical properties of the composites. These can be explained by the fact that BN has low Young's modulus, density and non-reactive nature as well as considerable anisotropy of many properties such as thermal expansion, thermal diffusivity/conductivity. Thus, the addition of BN in MgAlON is likely to lead to the presence of microcracks caused by the mismatch of thermal expansion coefficient. The microcracks result in the enhancement of the strength at elevated temperature and thermal shock durability of the composites.

Effective thermal conductivities were evaluated from the present experimental results of thermal diffusivities, heat capacity and density. A model suitable for present composites has been derived based on Luo's model. The predicted lines calculated by the model were in good agreement with experimental results.

The reactions between the composites and molten iron as well as the slag were investigated by ''finger'' experiments and sessile drop experiments. Both experimental results indicated that the BN addition has positive influence on the corrosion resistance. These are attributed to the excellent corrosion resistance of BN to molten iron and slag, such as the higher contact angle between BN substrate and liquid iron and molten slag compared with that obtained for pure MgAlON.

Keywords: MgAlON-BN composites, Mechanical properties, Thermal shock durability, Thermal diffusivity/conductivity, Corrosion resistance.

Acknowledgements

First, and most of all, I express my deepest and sincere gratitude to my supervisor Prof. Seshadri Seetharaman for giving me this opportunity to work in this active research group and giving me constant support and guidance during this work. It is his patience and continuous encouragement that made me a better, confident man, and become professional. In a word, I could not have accomplished the expertise I gained without his guidance.

I wish to express my gratitude and regards to Prof. Wenchao Li. You not only gave me the fruitful suggestions and guidance, but also gave me the chances to inquire into social intercourse experiences these years.

The author is grateful to Dr. Lidong Teng, Dr. T. Matsushita for their invaluable techniques, detailed discussions and constructive suggestions during this work.

I thank Docent Ragnhild E. Aune, Dr. Era Kapilashrami and Tech. Lic. Riad Abdul Abas sincerely for their detailed discussion and help during this work.

Mr. Peter Kling and Ms. Wenli Long are gratefully acknowledged for their detailed technical help and discussions during this work.

I am thankful to Prof. Xidong Wang and Prof. Mei Zhang for their continuous support received during these years. Prof. K. Mukai and Prof. K.C. Chou are acknowledged for their constructive discussions. I am obliged to associate Prof. JingJie Li for constant understanding and encouragement.

I thank Ms. Pengli Dong, Dr. Baijun Yan and Mr. Fan Li for the great help received during these years.

A special thanks to Mr Jun Zhang as a professional cook and helpful discussion as well as encouragement during the past year. Dr. Tuping Zhou, Qian Dong and Yanbing Cai are acknowledged for their help during the past years.

Ms. Shiye Zhao is acknowledged for constant criticism, encouragement and understanding. I also extend my sincere thanks to Mr. Haizhong Zhang and Ms. Xiaoheng Sun, my best friends, for constant help and understanding.

I thank all friends and colleagues working at Department of Materials Science and Engineering.

Finally, this thesis is dedicated to my parents for their love and support.

Zuotai Zhang

Stockholm February 2006

Supplements:

This thesis is based on the following papers:

1. ‘‘Synthesis and characterization of MgAlON-BN composites’’

Zuotai Zhang, Wenchao Li, Xidong Wang, Seshadri Seetharaman

Sent to Z. Metallkd for publication.

2. ‘‘Mechanical Properties and Microstructures of hot-pressed MgAlON-BN Composites’’

Zuotai Zhang, Lidong Teng, Wenchao Li

Sent to J. Eur. Ceram. Soc. For publication.

3. ‘‘Thermal shock Behavior of MgAlON and MgAlON-BN Composites’’

Zuotai Zhang, Lidong Teng, Wenchao Li and S. Seetharaman

Sent to J. Am. Ceram. Soc. for publication.

4. ‘‘Investigation of Wetting Characteristics of Liquid Iron on Dense MgAlON-based Ceramics by X-Ray Sessile Drop Technique’’

Z.T. Zhang, T. Matsushita, W.C. Li and S. Seetharaman

Metallurgical and Materials Transactions B, 2006, vol.37, In press.

5. ‘‘Thermal diffusivity/conductivity of MgAlON-BN Composites’’

Z.T. Zhang, W.C. Li and S. Seetharaman

Metallurgical and Materials Transactions B, 2006, In press.

6. ‘‘Reactions between MgAlON-BN composites and $CaO-SiO_2-Al_2O_3-MgO-$"FeO" slag’’

Z.T. Zhang, T. Matsushita, W.C. Li and S. Seetharaman

Sent to Metallurgical and Materials Transactions B for publication.

Other papers are not included in this thesis.

1. **Zhang Zuotai**, Saiyin Bater, Li Wenchao. Manufacture and properties of AlON-TiN particulate composites. Material and Design. 2005, 26: 363-368

2. **Zhang Zuotai,** Xidong Wang, Li Wenchao. Kinetic studies of oxidation of AlON-TiN composites. Journal of alloys and compounds, 2005, 387, 74-81

3. **Zuotai Zhang,** Xidong Wang, Mei Zhang and Wenchao Li. Synthesis and Characterization of γ-AlON-TiN composites. Key Engineering Material , vols. 280-283 (2005) pp.1133-1138

4. **Zhang Zuotai**, Saiyin Bater, Li Wenchao. Synthesis of AlON-TiN composites and optimization of the Synthesis technology. Journal of Chinese Ceramic Society, 2003, 8(31): 725~731

Table of contents

1. Introduction

Oxides are widely used as refractory materials. However, diversification and sophistication in the technology require the development of new refractories. Oxides have excellent corrosion resistance, but their thermal shock resistance is poor. The development of new high temperature technologies necessitates the development of new-generation refractories that can survive in extreme conditions-not only high temperatures and high heat fluxes, but also wear, chemical attack and mechanical loads[1]. In this case, some carbide, nitride and oxynitride such as SiC, Si_3N_4 and SiAlON have been expected to constitute new generation refractories in view of their unique combination of high hot strength, high thermal shock resistance and high corrosion resistance[2]. But the SiAlON and Si_3N_4 will decompose by the dissolution of silicon and nitrogen into molten steel[3]. In this case, MgAlON or its MgAlON-based composites can be expected to find application in high performance refractories.

Magnesium aluminum oxynitride (MgAlON) has been quite attractive as a high-performance ceramic material in view of its promising optical, mechanical and chemical properties, thus having the potential as a superior ceramic material at high temperature[4-6]. A number of investigations have shown that graphite-based refractories incorporating some MgAlON could improve the resistance to slag and steel corrosion. This indicates that MgAlON can be expected find application as high performance materials. To use ceramics as high performance materials, it is necessary to give a high durability for thermal shock and erosion, together with appropriate strength and toughness. In general, to improve the thermal shock resistance, materials need to have high thermal conductivity and low thermal expansion coefficient. Hexagonal boron nitride (h-BN) which demonstrates excellent thermal shock resistance and machinability may fulfil above-mentioned requirements in addition to its non-reactive nature[7]. These indicate that BN is a suitable candidate in developing a material with high resistance to oxidation and chemical attack as well as high thermal shock resistance by incorporation into other materials. Thus, MgAlON-BN composites are expected to find application in special refractory nozzles, tubes, break rings for the continuous casting of steel instead of Si_3N_4-BN[8] and Sialon-BN[9] composites. The present project was initiated with an aim to investigate the synthesis mechanism of MgAlON/BN composites and its physicochemical properties.

Mechanical properties indicating the capability of supporting load and compressive stress are important properties for high performance structural composite ceramics and advanced refractories. The mechanical properties are mainly determined by the microstructure of composite ceramics–the phase component and combination of grain boundary phases as well as the residual stress and microcracks in the composite ceramics[10,11]. Further, the wear and erosion of refractories in steelmaking process create serious problems, with implications on process economy and environment, since the wear and erosion are closely related with the mechanical properties of refractories. Therefore, it is necessary to investigate the relationship between mechanical properties and their microstructure.

The refractories in the metallurgical process come under severe attack by molten steel and slag. This attack generally consists of two types, that the chemical attack and mechanical erosion. In the case of the latter, the refractories are peeled off and the peeled pieces follow the flowing steel, leading to accumulation of oxide inclusions in the steel[12]. The resistance ‘‘peeling’’ properties can be characterized by thermal shock durability. Thus, it is necessary to study the thermal shock properties of refractory materials.

Chemical attack, as mentioned above, includes the reactions between refractories and molten steel and slag. Generally, molten steel contains a number of dissolved elements including carbon, oxygen and sulphur in very small quantities. Hence, the present project investigated the wetting characteristics between refractories and molten iron containing different oxygen contents. In addition, slag corrosion mechanism was studied in view of the importance of factors like refractory cost and the contamination of the metal due to non-metallic inclusions. In the present work, the mould slag was used for the investigations because MgAlON-BN composites are expected to find application in nozzles, tubes and break rings for continuous casting of steel.

2. Theoretical Aspects

2.1 Calculation of Gibbs energy of MgAlON

Several investigations have been reported on the synthesis parameters and phase diagrams of MgAlON ceramics[4,13,14]. Wang et al[4] assumed that MgAlON is a near-ideal solid solution of AlON and $MgAl_2O_4$ in view of the fact that MgAlON, $MgAl_2O_4$ and AlON have the same spinel structure and similar lattice parameters. These authors carried out the estimation of the Gibbs energy of MgAlON, and drew up the phase stability diagram of Mg-Al-O-N system at 2073 K[4].

The present author calculated the Gibbs energy of formation of MgAlON using the method proposed by Kaufman[15-21]. In the present work, the symbolic conventions of Kaufman are used, i.e. Al_2O_3 was labeled as AO, MgO as MO and AlN as AN. The binary systems, such as Al_2O_3-MgO and Al_2O_3-AlN, have been calculated, thus the extension to quasi-ternary systems can be readily accomplished on the basis of calculated binary system in Reference[17,18]. MgAlON was synthesized by the reaction between Al_2O_3, AlN and MgO[4,6], which can be represented by Eq. (1):

$$0.7Al_2O_{3(s)} + 0.2AlN_{(s)} + 0.1MgO_{(s)} = Mg_{0.1}Al_{1.6}O_{2.2}N_{0.2(s)}\,(AO_{0.7}AN_{0.2}MO_{0.1}) \qquad (1)$$

where AO, AN, MO are (1/5)Al_2O_3, (1/2)AlN and (1/2)MgO respectively.

Then, the Gibbs energy, G^s, of a compound phase $AO_{0.7}AN_{0.2}MO_{0.1}$ is defined by means of Eq. (2) as follows[16,17]:

$$G^s = 0.7^o G^S_{AO} + 0.20^o G^S_{AN} + 0.10^o G^S_{MO} + (0.70)(0.20)(0.90)^{-1}(0.70LAOAN + 0.20LANAO - C(T)) + (0.70)(0.10)(0.80)^{-1}(0.70LAOMO + 0.10LMOAO - C(T)) + (0.20)(0.10)(0.30)^{-1}(0.20LANMO + 0.10LMOAN - C(T))J \cdot g^{-1} \cdot at^{-1} \qquad (2)$$

In this equation, the first three terms are the Gibbs energy terms corresponding to pure AO, AN and MO in the spinel structure for the compounds under consideration. The subscript ‘‘s’’ stands for the spinel phase. LAOAN and other terms are interaction parameters that are functions of temperature but not of composition. C(T) (which is a temperature dependent function) is the compound parameter. The stability parameters for these phases are defined along the lines proposed by Kaufmann[17-21] as well as Willems[16].

$LANMO = LMOAN = LAOAN = LANAO = 29288 J \cdot g^{-1} \cdot at^{-1}$ from reference[15].

LAOMO=-33530+22.93T, LMOAO=59910-27.11T $J \cdot g^{-1} \cdot at^{-1}$ from reference[19], and the compound parameters for this phase is C(T)=120081-12.678T $J \cdot g^{-1} \cdot at^{-1}$

Thus,

$$G^s = 0.7^o G^S_{AO} + 0.20^o G^S_{AN} + 0.10^o G^S_{MO} + (-23258.09 + 3.98245T) J \cdot g^{-1} \cdot at^{-1}$$

Then the Gibbs energy change for the reaction,

$$0.14 Al_2O_{3(C)} + 0.1 AlN_{(N)} + 0.05 MgO_{(P)} \rightarrow [0.14 Al_2O_3 \bullet 0.1 AlN \bullet 0.05 MgO](SP)$$

$$\Delta_f \mathrm{G}^\Theta = 0.7\left({}^{\mathrm{o}} G^S_{AO} - {}^{\mathrm{o}} G^C_{AO}\right) + 0.2\left({}^{\mathrm{o}} G^S_{AN} - {}^{\mathrm{o}} G^N_{AN}\right) + 0.1\left({}^{\mathrm{o}} G^S_{MO} - {}^{\mathrm{o}} G^P_{MO}\right) + (\text{-}23258.09 + 3.98245\mathrm{T}) \quad (3)$$

where the subscripts ‘‘C’’ is corundum form of Al_2O_3, ‘‘N’’ is hexagonal form of AlN, and ‘‘P’’ is periclase of MgO.

In Eq. (3),

$${}^o G^S_{AO} - {}^o G^C_{AO} = AOAOSC = AOAOLS - AOAOLC = -4435 + 1.123T \quad (4a)$$

$${}^o G^S_{AN} - {}^o G^N_{AN} = ANANSN = ANANLS - ANANLN = 42593 - 4.94T \quad (4b)$$

$${}^o G^S_{MO} - {}^o G^P_{MO} = MOMOSP = MOMOLS - MOMOLP = -28138 + 4.94T \quad (4c)$$

Where AOAOSC is used to designate the Gibbs energy of spinel form of Al_2O_3 minus the Gibbs energy of corundum form of Al_2O_3, ANANSN is the Gibbs energy difference between spinel form of AlN and hexagonal form of AlN, and MOMOSP is the Gibbs energy difference between spinel form of MgO and periclase form of MgO.

Thus, substituting Eq. (4a-c) into Eq.(3), the Eq.(5) can be obtained:

ΔG=-20657.7+4.27T $J \cdot g^{-1} \cdot at^{-1}$

Therefore,

$\Delta_f G^\Theta(\mathrm{Mg_4Al_{29}O_{43}N_3})$=-1631958.3+337.33 $J \cdot mol^{-1}$ (5a)

$$\Delta_f G^\Theta(MgAl_{16}O_{22}N_2) = -846965.7 + 175.07 J \cdot mol^{-1} \quad (5b)$$

These expressions are used in the following calculation.

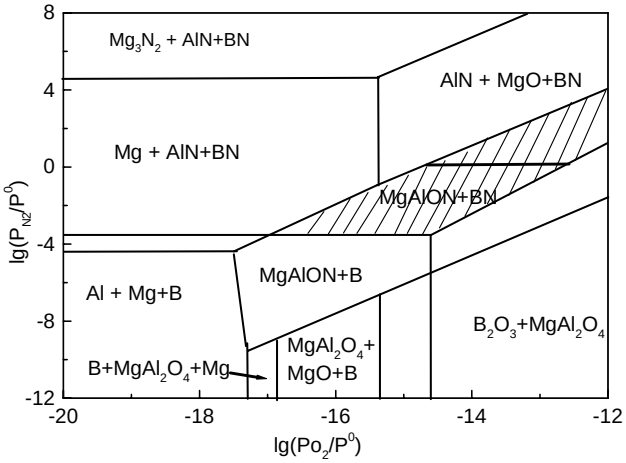

Figure 1. Phase stability diagram of Al-Mg-O-N and B-O-N systems

During the synthesis of MgAlON-BN composites, the related possible chemical reactions at 1800 ^{o}C except for Al_2O_3-AlN-MgO system are listed as follows:

$$B_{(l)}+N_2=2BN_{(s)} \quad (6)$$

$$\lg(\frac{p_{N_2}}{p^{\Theta}}) = -3.52$$

$$4B_{(l)}+3O_2=2B_2O_{3(l)} \quad (7)$$

$$\lg(\frac{p_{o_2}}{p^{o}}) = -13.3$$

$$4BN_{(s)}+3O_2=2B_2O_{3(l)}+2N_2 \quad (8)$$

$$\lg(\frac{p_{N_2}}{p^{\Theta}}) = -1.5\lg(\frac{p_{O_2}}{p^{\Theta}}) + 18.45$$

A combined phase stability diagram for the systems Al-Mg-O-N and B-O-N is drawn on the basis of the above calculations and is shown in Figure 1. As can be seen in this figure, MgAlON and BN have the same homogeneity region, and the proper control of the atmosphere is essential for the synthesis MgAlON-BN composites. At 2073 K, and at a given nitrogen pressure of 101325 Pa, oxygen pressure should be controlled between about 10^{-8} to 10^{-10} Pa.

2.2 XRD quantitative analysis

A Matrix-flushing method proposed by Frank and Chung[22] was employed in the quantitative XRD analysis for the multi-component samples. When the monochromatic

primary X-rays impinge on a flat powder specimen, the intensities of diffracted rays are related to the percentage composition by the following equation,

$$w_i = (\frac{I_s^o}{I_i^o})_{1:1}(\frac{I_i}{I_s})\frac{w_w}{1-w_s} = K_i^s(\frac{I_i}{I_s})\frac{w_s}{1-w_s} \quad (9)$$

where:

w_s =Weight fraction of matrix-flushing agent.

w_i =Weight fraction to be measured in the multi-component samples.

I_i =intensity of X-rays diffracted by a selected plane (hkl) of component i.

I_s =intensity of X-rays diffracted by a selected plane (hkl) of matrix-flushing agent.

K_i^s =Reference Intensity ratio. For a binary mixture of compound ‘‘j’’ and reference sample ‘‘s’’ which is chosen for Reference Intensities at one-to-one weight ratio, then K_i^s can be obtained by the following equation:

$$K_i^s = (\frac{I_i}{I_s})_{1:1} \quad (10)$$

In the present study, silicon powder was chosen for the matrix-flushing agent, and h-BN for reference sample due to its stability under C or CO atmosphere. The mass ratio of silicon to the sample powder was taken as much as one third. The sample powder and silicon powder were thoroughly mixed in agate mortar with alcohol solvent as the mixing agent and dried to form composite sample. Room temperature X-ray measurements of composite samples were carried out. The parameters involved were the receiving slit, 0.15mm, divergence slit and scatter slit, 0.1º, graphite crystal monochromator. Intensity was collected by 2θ scanning from 25º to 40º (2θ) with steps of 0.01º and rate of 1º/min. The fraction values were determined using the peak of (100) of h-BN and peak of (111) Si.

2.3 Thermal shock parameters

A number of thermal shock parameters have been defined in the past decades[23,24]. In general, two different approaches are adopted to derive the thermal shock parameters. The first approach is based on a fracture resistance consideration in which thermoelastic theories are used and the attention is focused on the initiation of fracture because of the thermal stresses. The R, R' and R'' parameters are thus derived as the following equations,

$$R = \frac{\sigma_f (1-v)}{E\alpha} \tag{11}$$

$$R' = \frac{\sigma_f (1-v)k}{E\alpha} \tag{12}$$

and $$R'' = \frac{\sigma_f (1-v)\Phi}{E\alpha} \tag{13}$$

where σ_f is the three point bending strength, E is the Young's modulus, α is the thermal expansion coefficient, v is the Poisson's ratio, k is the thermal conductivity, and Φ is a stress reduction term. The parameter R is applicable for the case of an instantaneous change in surface temperature under conditions of rapid heat transfer. R' is for a relatively slow heat transfer, and R'' is for a constant heating or cooling rate.

The second approach to determine the thermal shock resistance of materials is focused on the crack propagation and the resulting changes in the physical properties of the material. In this case, two parameters for damage resistance R''' and R'''' are defined by Hasselman as following[46,47],

$$R''' = \frac{E}{\sigma_f^2 (1-v)} \tag{14}$$

$$R'''' = \frac{E\gamma_{wof}}{\sigma_f^2 (1-v)} \tag{15}$$

where γ_{wof} is the effective surface energy or work of fracture per unit projected area of fracture face. The R''' parameter gives information about the minimum in the elastic energy at fracture available for crack propagation, and the R'''' parameter is the minimum in the extent of crack propagation on initiation of thermal stress fracture. For typical refractory materials, the initial strength may be low, but may have a significant resistance to crack propagation or extension caused by thermal shock. Thus, it is necessary to predict the thermal shock durability by calculating R''' and R'''' for refractories[25,26].

2.4 Temperature dependence of thermal diffusivity/conductivity

Generally, thermal conductivity is determined by lattice vibration (phonon conduction) in insulators. Debye proposed that the thermal conductivity of insulator λ can be described as the following equation using kinetic theory of gases[27,28],

$$\lambda = \frac{1}{3} C_v v l \tag{16}$$

where C_v is the heat capacity at constant volume in $J/K \cdot m^3$, v the velocity of sound and l the phonon mean free path. Eq. (16) can be combined with $\lambda = \alpha \rho C_p$. If the thermal expansion can be neglected for the solid state, then relationship $C_v = \rho C_p$ can be used to deduce the following equation[28],

$$\alpha = \frac{1}{3} vl \tag{17}$$

If it is assumed that the v is constant irrespective of temperature, the thermal diffusivity is proportional to the phonon mean free path. The phonon mean free path ''*l*'' is limited by collisions with other phonons and with lattice defects of various kinds. These mechanisms can be assumed as additive[27],

$$\frac{1}{l_{tot}(q,s)} = \frac{1}{l_{ph-ph(q,s)}} + \sum \frac{1}{l_{ph-def(q,s)}} \tag{18}$$

where the first term on the right hand side refers to phonon-phonon collisions and the next terms to phonon scattering by faults such as points defects, dislocations, grain and phase boundaries as well as finite size of the sample. Generally, above room temperature, phonon collisions that limit the thermal conductivity must involve three or more phonons, and these process lead to phonon mean free path *''l''* is proportional to $\frac{1}{T}$(mainly for three phonon processes), or l~$\frac{1}{T^2}$ for four phonon processes. $l_{ph-def(q,s)}$ is independent of temperature. Thus, the thermal diffusivities are expected to decrease with increasing temperature. At very high temperatures, the mean free path cannot be shorter than a characteristic distance between two neighbouring atoms, these lead to the thermal diffusivity decrease very slowly with increasing temperature at very high temperatures.

2.5Surface reactions

2.5.1 Thermodynamic analysis of Mg-Al-O-N-Fe-B systems

To understand the mechanism of wetting characteristics of oxygen-containing iron on substrate, it is necessary to understand the reactions between substrates and liquid iron under purified argon gas as well as different oxygen partial pressures. In the present experiment, a thermodynamic study involving Mg-Al-O-N-B-Fe system imposed on P_{O_2} was carried out. After introduction of Ar, CO and CO_2 gas mixtures, the reaction equations can be written as follows,

$$MgAl_{15}O_{19}N_3 + 2.25O_2 = 6.5Al_2O_3 + MgAl_2O_4 + 1.5N_2 \quad (19)$$

$$\frac{4}{3}BN_{(s)} + O_{2(g)} = \frac{2}{3}B_2O_{3(l)} + \frac{2}{3}N_{2(g)} \quad (20)$$

$$2Fe(l) + O_2 = 2FeO(l) \quad (21)$$

$$Fe + Al_2O_3 + \frac{1}{2}O_2 = FeAl_2O_4 \quad (22)$$

$$2Al_2O_3 + B_2O_3 = Al_4B_2O_9 \quad (23)$$

$$(1-x)MgO + xFeO = Mg_{1-x}Fe_xO \quad (24)$$

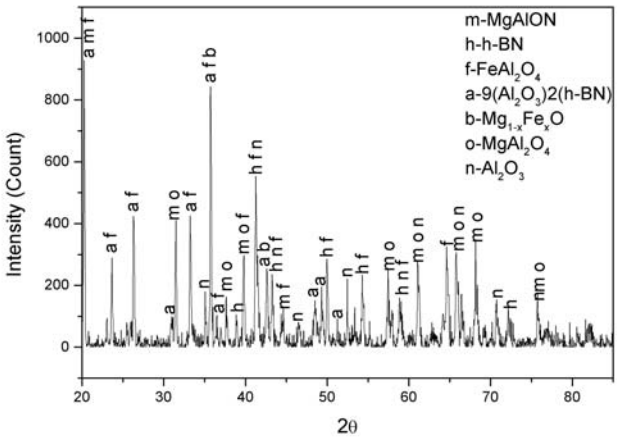

Figure 2. XRD analysis of surface of MgAlON-30vol%BN composite after experiment at an oxygen pressure, P_{O2}=1,5×10^{-2}Pa

The substrates would be oxidized when the gas atmosphere was changed from purified argon gas to the P_{O_2} values imposed. The oxidation products of substrate are Al_2O_3, B_2O_3, $MgAl_2O_4$ and $(Al_2O_3)_9(B_2O_3)_2$. It should be pointed out that B_2O_3 could not be detected by XRD, and oxidation products would combine FeO to form $FeAl_2O_4$ and $Mg_{1-x}Fe_xO$ at the experimental temperature. This was verified by XRD analysis shown in Figure 2. The products would form a ternary FeO-MgO-Al_2O_3 or a quaternary slag by combining with B_2O_3. The above result is in agreement with the results of SEM-EDS analyses.

2.5.2 Reactions between MgAlON and mould slag

As the specimen rod was dipped into molten slag, chemical reactions would take place between sample and components in slag. The composition of $MgAl_{16}O_{22}N_2$ used in the present experiment is not thermodynamically stable under the experimental temperature.

It is likely to decompose into $MgAl_{(16-3x)}O_{(22-3x)}N_{(2-x)}$, AlN and Al_2O_3[29]. The AlN formed is easily combined with some MgO in the slag to form Mg_3N_2. The sublimation and decomposition temperatures of Mg_3N_2 are only 700°C and 800°C in vacuum conditions, respectively[47], thus the volatilization should be especially severe at the experimental temperature, which may provide the source of gas bubble generation[18]. In the case of the slag composition used in the present experiment, the Al_2O_3 and MgO are not saturated in the slag, and consequently MgAlON is likely to react with the components in the slag to generate some gehlinite, akermanite and anorthite as well as AlN during the reaction process. Therefore, the representative reactions between MgAlON and slag may occur as follows,

$$MgAl_{16}O_{22}N_2 = MgAl_{(16-3x)}O_{(22-3x)}N_{(2-x)} + xAlN + xAl_2O_3 \quad (25)$$

$$\mathrm{MgAl_{16}O_{22}N_2 + 2CaO + 2SiO_2 = Ca_2MgSi_2O_7 + 7Al_2O_3 + 2}Al\mathrm{N} \quad (26)$$

$$\mathrm{MgAl_{16}O_{22}N_2 + CaO + 2SiO_2 = CaAl_2Si_2O_8 + MgAl_2}O_4 + 5Al_2O_3 + 2Al\mathrm{N} \quad (27)$$

$$\mathrm{MgAl_{16}O_{22}N_2 + 2CaO + SiO_2 = Ca_2Al_2SiO_7 + Mg}Al_2O_4 + 5Al_2O_3 + 2AlN \quad (28)$$

$$2AlN + 3MgO = Mg_3N_2 \uparrow + Al_2O_3 \quad (29)$$

$$\mathrm{nAl_2O_3 + MgO = Mg}O \cdot nAl_2O_3 \quad (30)$$

$$SiO_2 + Al_2O_3 + 2CaO = Ca_2Al_2SiO_7 \quad (31)$$

Thus, the continuous gas bubbles generation during the progress of the corrosion of MgAlON by molten slag is mainly caused by the volatilization of reaction products between MgAlON and molten slag.

3 Experimental methods

In the present thesis, five experimental methods were employed to investigate the physicochemical properties of MgAlON-BN composites involving mechanical properties, thermal shock properties and thermophysical properties.

3.1 Synthesis methods and Mechanical properties measurement

This forming technique is the simultaneous application of external pressure and temperature to enhance densification. It is conducted by placing either powder or a compacted preform into a suitable die, typically graphite, and applying uniaxial pressure, while the entire system is held at an elevated temperature, e.g. 2000°C for SiC. Figure 3

presents the schematic diagram of hot pressing unit. The present experiment was carried out at 2073 K at 20MPa under N_2 atmosphere. The holding time was 2 hours.

The hot-pressed composites were cut into 3mm×4mm×40mm strips perpendicular to the hot-pressing direction, then the three point bending method was introduced to measure room temperature bending strength[30]. Fracture toughness was measured using the single edge notched beam (SENB) technique, with a notch cut using a 1 mm thick diamond blade producing a notch to depth ratio of 0.25 compared with height, the loading rate being 0.5mm/min[31]. The Vickers hardness (H_v) of the composites was calculated from the average results of five indentations performed under a load of 98 N on a polished surface of the sample.

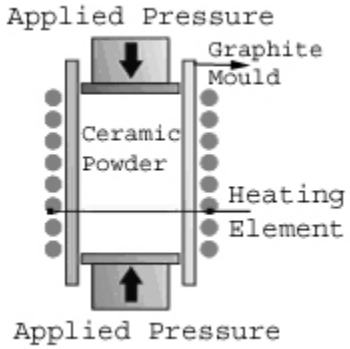

Figure 3. A schematic diagram of hot pressing unit

3.2 Thermal shock experiment

To use composites as engineering material, it is necessary to give a high durability for thermal shock together with appropriate strength and toughness. For this purpose, the thermal shock experiment was conducted. Thermal shock durability was characterized using the retained strength after the experiment. The experiments were performed in a vertical tube furnace in argon atmosphere. Specimens were held in the furnace for 30 minutes to allow for temperature equilibration at different temperatures followed by dropping them into a container of water at $15\pm5^{o}C$. Tests were carried out in the thermal shock temperature range range of $400^{o}C$ to $1500^{o}C$. The samples after thermal shock experiments were cleaned with acetone, and then dried at $100^{o}C$ for 5 hours. The retained strength of the specimens before and after the water quenching was measured using a three point bending method. The standard equations for the strength (σ_f) of a bar in three point bending method can be described as follows[30],

$$\sigma_f = \frac{3}{2} \times \frac{PL}{bw^2} \tag{32}$$

where P is the load at fracture, L is the length of support span, b is the specimen width, w is the specimen thickness.

3.3 Laser flash and DSC methods

Thermal conductivity is one important characteristics for engineering composites. It determines the thermal shock properties. Thus, the thermal conductivity was calculated by multiplying the thermal diffusivity and heat capacity as well as density in the present experiment. The measurements of the thermal diffusivity, α, were performed with a laser flash device (Model TC-7000H/MELT Ulvac-Riko). Figure 4 gives the schematic diagram of the laser flash unit. In the process of measuring, the top surface of the disk sample is irradiated with a laser which provides an instantaneous energy pulse. The laser energy is absorbed on the top surface of a sample and gets converted into the heat energy. The heat energy conducts through the sample. Immediately after the laser pulse, the temperature of the rear surface of the sample is monitored by collecting the radiation using a photovoltaic infrared detector. The signal from the detector is amplified and sent to a computer for analysis. The thermal diffusivity, α, is obtained from the Eq. (33) [28],

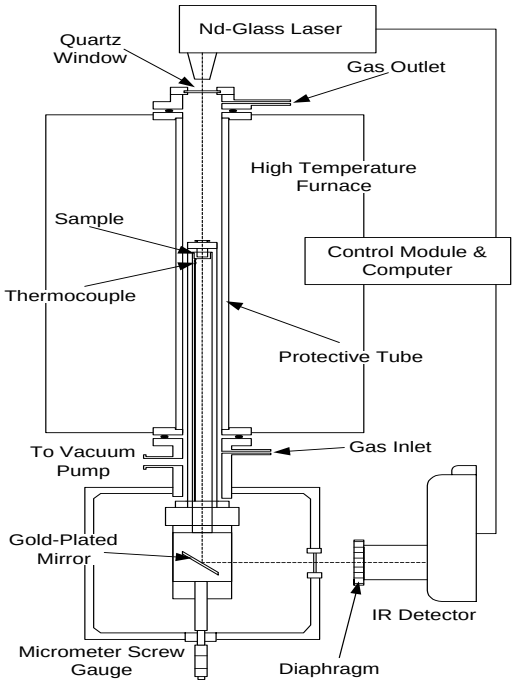

Figure 4. A schematic diagram of the laser flash unit

$$\alpha = \frac{1.37 \bullet L^2}{\pi^2 \bullet t_{1/2}} \tag{33}$$

where L is the thickness of the sample and $t_{1/2}$ is the time required for the temperature of the rear surface to reach half of its maximum temperature. The thermal diffusivity measurements were carried out during the heating cycle at first and then during the cooling cycle.

The measurements of the heat capacity were performed with a differential scanning calorimeter (DSC) from Netzsch STA 449C Jupiter unit. The experimental procedure has been described earlier in the present laboratory[32], and is briefly outlined here. The calorimeter covers a temperature range 25-1400^oC. The measurements were performed in a platinum crucible with a platinum lid on the top. One sapphire disk was positioned between the measuring head and the platinum crucible. The crucible, sapphire disk and lid were marked in order to ensure that these were always in the same position for each run. The same type of platinum disk and lid were used as the reference. A type S thermocouple was connected to the measuring head. The reaction chamber was evacuated three times before the measurements started. Argon gas (<5ppmO_2) supplied by AGA Gas AB in Stockholm was used to protect the sample and balance. The argon gas was purified by passing through columns of silica gel and dehydrate to absorb the moisture, through ascarite to remove carbon dioxide, and through tube furnaces containing copper and magnesium at 600^oC and 500^oC respectively to remove residual oxygen.

The furnace was stabilized at 40^oC for 20 minutes before heating to 1300^oC at a heating rate of 10^oC /min according to a predetermined temperature program. The standard run was conducted with a 1 mm thick sapphire disc provided by Netzsch Instruments, UK. The calibration files of the DSC apparatus including temperature file and sensitivity file were corrected by checking the melting points of five different metals and their enthalpies of transformation. The heat capacities of the composites were calculated by Netzsch Thermal Analysis software for MS windows. Parts of the experiments were repeated to confirm the reproducibility of the results.

3.4 X-ray sessile drop method

X-ray sessile drop method was conducted to investigate the reactions between the composites and molten iron or molten slag at different temperatures. The reaction process was monitored by the change of contact angle for molten iron and the variation numbers

of gas bubbles for molten slag. These investigations were expected to provide useful information as to the reaction mechanism at micro level. The experiments were carried out under continuous changing conditions. Thus, the surface tension of the iron drop or molten slag could therefore not be measured.

The sessile drop apparatus consists of a high temperature furnace and a Philips BV-26 mobile imaging system with an X-Ray source of 40-105 kV power. The furnace assembly which was supplied by Thermal Technology Inc with a maximum temperature 2300 K was equipped with a graphite heating element. The furnace was fitted with an alumina reaction tube. The temperature of the furnace was controlled by a Eurotherm temperature regulator within ±2 K. There were two parallel ports in the furnace assembly with quartz windows that allow the passage and detection of X-rays from the Philips BV X-ray unit. The imaging system consisted of a CCD camera with digital noise reduction. The image acquisition card enabled the recording of the X-Ray image at a maximum rate of 30 frames per second. The system could be used under vacuum, inert gas, or with gas mixtures.

The pure iron rod with a mass of about 1 gram was placed in the furnace. All handling was done with the aid of tweezers to avoid contamination. The upper surface of the sample was levelled carefully before the furnace assembly was closed. The system was evacuated to about 10^3 Pa. The reaction tube was then filled with argon gas for approximately 12 hours in order to flush the system completely. The furnace was heated to the preset temperature above the melting point. After this temperature was reached, the furnace was stabilized for about 0.5 h. In the case of experiments under pure argon gas atmosphere, 5 different temperatures were used, and at each temperature, the furnace was stabilised for 30 minutes. X-ray images were taken at each temperature in static mode using three different X-ray source power. The flow rate of argon gas was 0.140 L/min. In the case of the experiments at different oxygen partial pressures, gas mixtures of CO-CO_2-Ar with preset ratios were introduced into the system. Once the gas mixtures were introduced into the system, X-ray images were taken at regular intervals in video mode. At the end of the experimental run, CO and CO_2 were stopped and the furnace was shut down. The substrate was taken out at room temperature and the surface was examined by X-Ray diffraction. The substrate was then cut along the contact part with iron drop. The cross section was examined by scanning electron microscope (SEM) analysis. Some selected experiments were repeated in order to confirm the reproducibility of the results.

Gas bubbles generation experiment was carried out in the same apparatus, and the experimental procedure was similar as mentioned above. A piece of the synthetic slag rod with a mass of about 0.5 gram was placed in the furnace. The furnace was evacuated three times, and was then flushed with argon gas for 12 hours. The furnace was heated to the required temperature and X-ray images were then taken at each temperature in static mode using three different X-ray source power. The flow rate of purified argon gas was 0.140 L/min. In order to verify the reliability of the experiment, some experiments were repeated. The results were in good agreement with each other.

3.5 Slag corrosion test

Slag penetration experiment was conducted by immersing the composite rod into synthetic molten slag corresponding to the mould slag composition. The purified argon gas was used in this experiment. The experimental details and procedure are presented in supplement 6, and is briefly outlined here. The iron crucible containing the synthetic slag was placed in the heating zone of the furnace. The specimen rod clamped by a sample holder was positioned slightly above the crucible. The reaction tube was then filled with argon gas for approximately 12 hours in order to flush the system completely. The furnace was heated to the pre-set temperature. After the attainment of this temperature, the furnace was stabilized for about 4 hours to obtain the homogeneous slag, and then the sample was immersed into the slag for a given time. After the required reaction time, the sample was pulled out and allowed to cool in the argon gas atmosphere. The sample was then cut, ground, polished and examined using optical microscope as well as scanning electron microscope (SEM) equipped with energy dispersive spectroscope (EDS) analysis. The optical microscope was used to measure the radius of specimen rod. The error associated with this analysis was estimated to be ±0.05mm.

4 Results

4.1 Crystal characteristic analysis of MgAlON-BN composites

The MgAlON-BN ceramic materials with different compositions fabricated by hot pressing method in this experiment were investigated by X-Ray diffraction analysis. Some of the results are shown in Figure 5. As can be seen from above figures, the main phase is MgAlON, the second is h-BN and no impurities are found. All the peaks of

MgAlON could be indexed as a cubic cell, and BN was a hexagonal cell. The results in

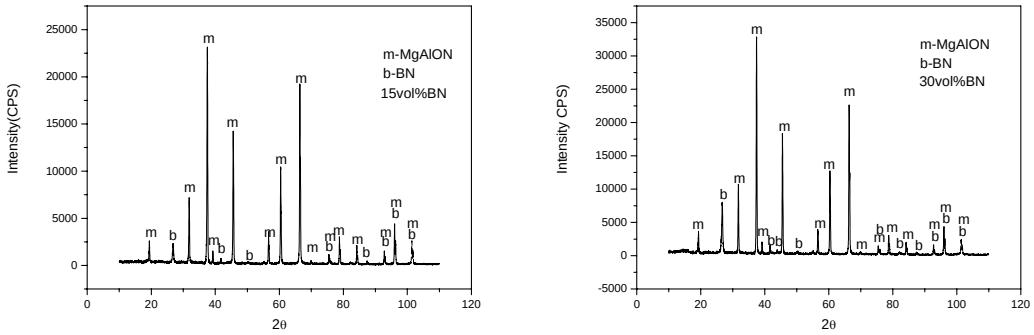

Figure 5. XRD patterns of MgAlON-BN composites

the case of the samples were found to be similar. The fracture section morphologies of MgAlON-BN with different compositions were investigated by SEM. Some results are shown in Figure 6. It is observed from the SEM photographs that the equiaxed grains are MgAlON, and the rod-like or flake-like grains are BN. BN particles are dispersed on grain boundaries. TEM results show the same pattern. HREM was further used to analyze the interfaces of crystal grains for MgAlON-15vol%BN composite. The results shown in Figure 7(a) indicate that there is no glass phase existing between the grain boundaries of MgAlON, and the grains of MgAlON are bonded directly. Some glass phase, however, is located at the triple junction nodes between MgAlON and BN grains, as can be seen from Figure 7(b). EDS analysis of the glass shows that it is rich boron and oxygen. This can be explained by the fact that BN absorbs some oxygen to yield B_2O_3 during the synthesis process.

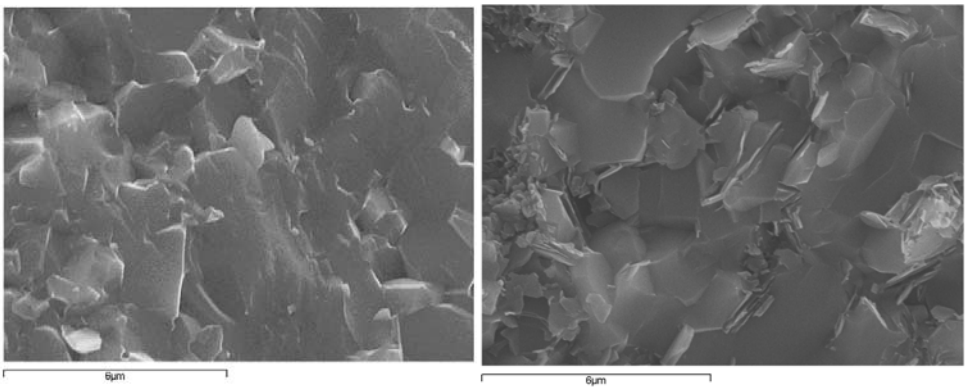

(a) (b)

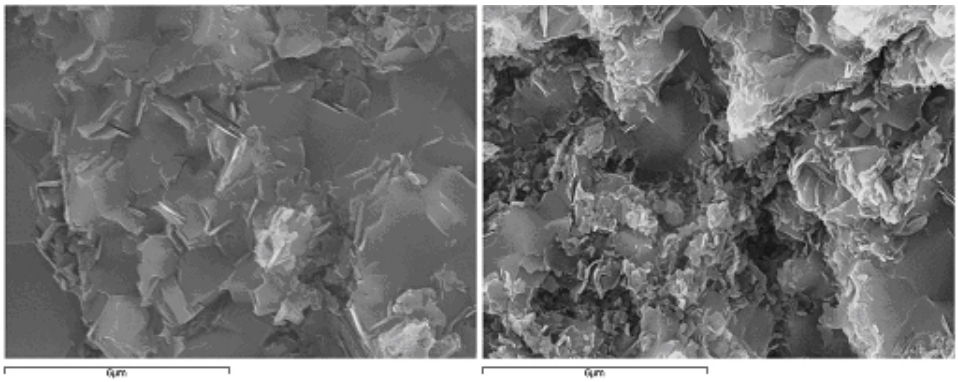

(c) (d)

Figure 6. SEM morphology of MgAlON-BN containing (a)MgAlON (b)10vol% (c)15vol% and (d) 30vol%

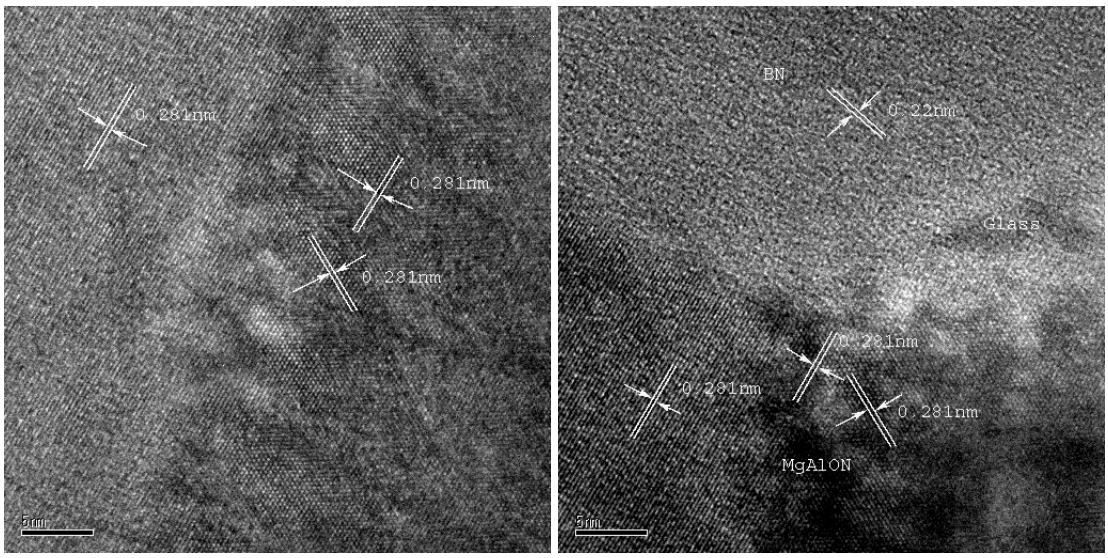

(a)MgAlON/MgAlON (b)MgAlON/BN

Figure 7. HREM images of MgAlON/MgAlON(h-BN) interfacs.

4.2 Mechanical properties of MgAlON-BN composites

The effect of h-BN addition on Vickers hardness, relative density, room temperature bending strength and fracture toughness of MgAlON/h-BN composites were investigated. Figure 8(a) shows Vickers hardness and relative density of the composite ceramics sintered at $1800^{o}C$ for 2h as a function of h-BN volume content. The Vickers hardness and relative density of MgAlON/h-BN composite ceramics decrease with an increase of h-BN volume fraction. The Vickers hardness of MgAlON/h-BN with 15% h-BN volume fraction is as high as H_V=6.82 GPa, which matches the requirements for machining [34,35]. Figure 8(b) shows room temperature bending strength and fracture toughness of

samples sintered at $1800^{o}C$ for 2 h as a function of h-BN volume fraction. The room temperature bending strength of MgAlON/h-BN composites decrease with an increase of h-BN volume fraction due to the inactive nature of h-BN. However, the fracture toughness of MgAlON/h-BN composites increase with increasing of h-BN content, reaching the maximum for 3.64 MPa·m$^{1/2}$, and then decrease considerably.

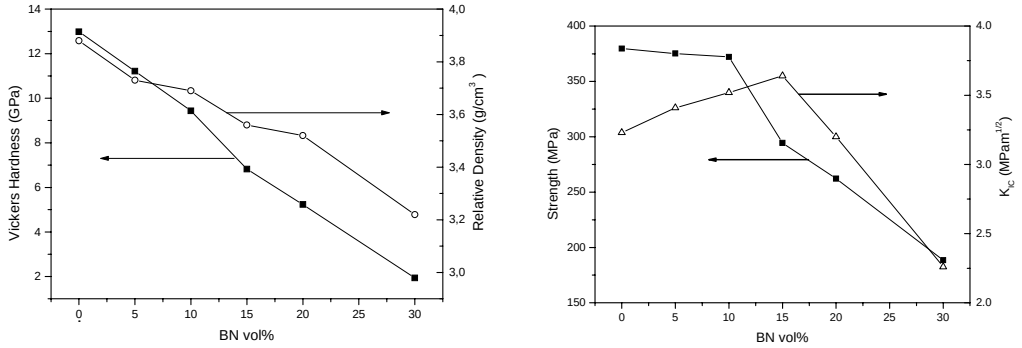

(a) (b)

Figure 8. Mechanical properties of MgAlON-BN composites as functions of BN contents

Figure 9 shows the temperature dependence of bending strength of MgAlON/15vol %h-BN in argon gas. As can be seen, bending strength increases with increasing temperature and reaches a maximum of 325.3 MPa at $800^{o}C$, then decreases to 231.1 MPa at $1200^{o}C$.

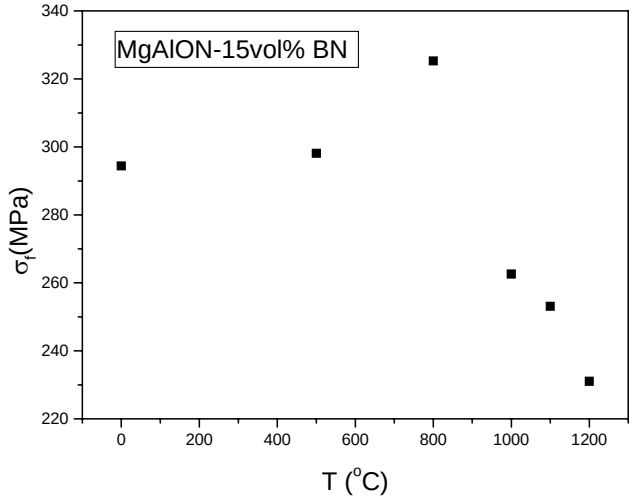

Figure 9. Temperature dependence of bending strength of MgAlON-15vol%BN sample in argon gas atmosphere

4.3 Thermal shock properties

Figure 10(a) shows the effect of single thermal shock on the strength of MgAlON and MgAlON-15vol%BN composites. It can be separated into two stages with increasing of thermal shock temperature difference(ΔT). Initially, the strength of MgAlON and MgAlON-15vol%BN composites remains constant for a substantial temperature range. The second stage is corresponding to the strength degradation. Figure10(b) gives the fraction of retained strength as a function of temperature differences. As can be seen, the fraction of retained strength are 37% and 53% for MgAlON and MgAlON-15vol% composites respectively after thermal shock difference $1500^{o}C$, i.e. MgAlON-15vol%BN composite materials show a better thermal shock resistance than that of MgAlON. Figure11 gives the surface morphology for MgAlON and MgAlON-15vol%BN composites after thermal shock experiment from ΔT =440℃ and 1500℃, respectively. No obvious cracks are found after thermal experiment from ΔT =$440^{o}C$ for both composites, and there are some obvious linking cracks on the surface of MgAlON, but no obvious cracks are found by SEM for the MgAlON-15vol%BN composites after thermal shock experiment from ΔT =$1500^{o}C$. Similar phenomena are observed in the cross sections for MgAlON and MgAlON-15vol%BN from ΔT =$1500^{o}C$. It should be pointed out that the samples were oxidized after thermal shock experiment from ΔT =$1500^{o}C$.

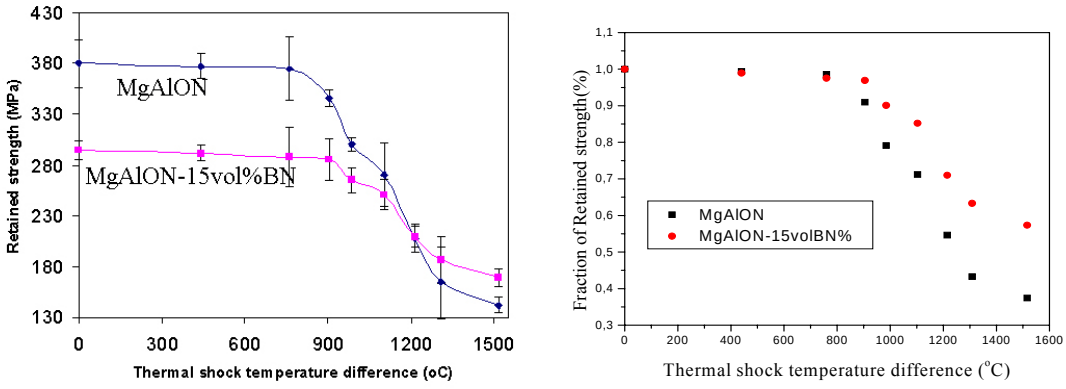

(a) (b)

Figure 10. Retained strength(a) and Fraction retained strength(b) as a function of thermal shock temperature difference(single thermal shock), for MgAlON and MgAlON-15vol%BN composites

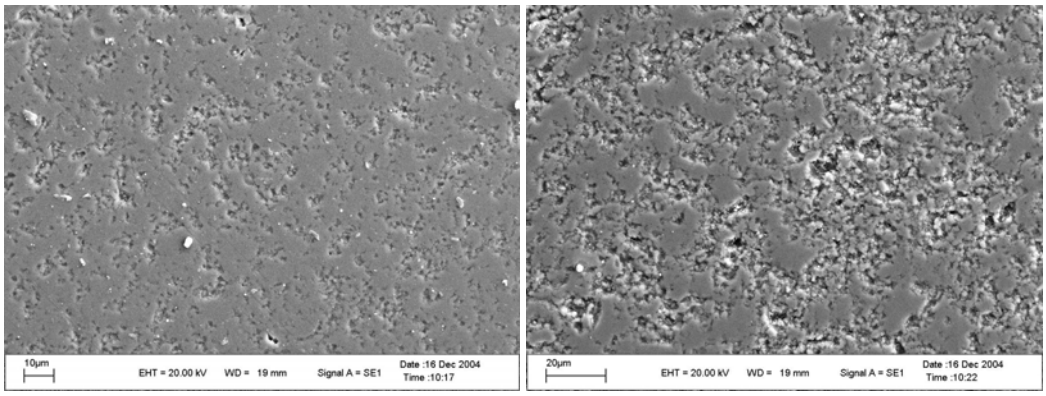

(a)MgAlON (ΔT =440℃) (b)MgAlON-15vol%BN

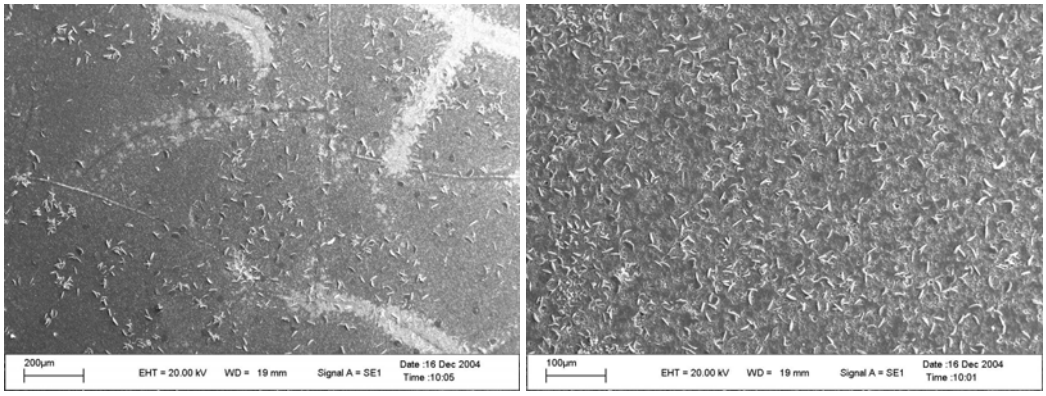

(c)MgAlON (ΔT =1500℃) (d)MgAlON-15vol%BN

Figure 11. Surfaces morphology for (a)(c)MgAlON and (b)(d)MgAlON-15vol%BN samples after thermal shock experiment from ΔT =440℃ and 1500℃

4.4 Thermal conductivity

Figure 12 shows the thermal diffusivities as a function of temperature both parallel to and perpendicular to the hot-pressing directions. The experimental results indicate that thermal diffusivities decrease quickly below $900^{o}C$, followed by a slow decrease with further increasing of temperature. Addition of BN particles has a significant influence on the thermal diffusivities, and results in the anisotropy properties of the composites with respect to the hot-pressing direction. The addition of BN increases the thermal diffusivities in both hot-pressing directions.

The heat capacity measurements were carried out in present paper, which showed a similar behaviour for all composites. The heat capacities increase with increasing

temperature below $900^{o}C$, and the slope for heat capacity curves is small with further

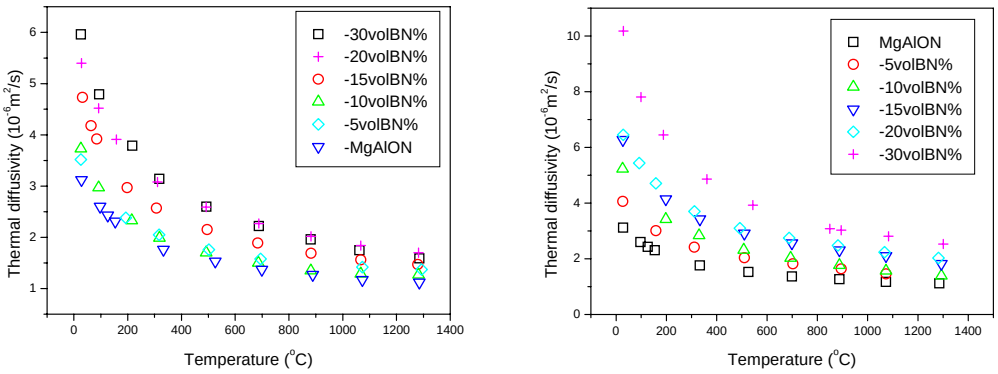

(a) (b)

Figure 12. Temperature dependent of thermal diffusivity of MgAlON with different BN contents. (a) parallel to hot-pressing directions. (b) perpendicular to hot-pressing directions

temperature increase. Addition of BN particles has a small effect on the heat capacity.

Effective thermal conductivities were thus calculated from the present experimental results of thermal diffusivities, heat capacity and density by the following equation[27]:

$$\lambda = C_p \rho \alpha \tag{34}$$

where C_p is the specific heat capacity and ρ is the density. It should be pointed out that the density of the composites at room temperature was used in the calculation of thermal conductivity because that the decrease of density is less than 0.5% from room temperature up to 1300°C. Figure 13 presents the computed effective thermal conductivities. As can be seen, the effective thermal conductivities decrease quickly with increasing temperature followed by a slow decrease at higher temperatures, the trend being the same as the thermal diffusivities of composites. The addition of BN has obvious effect on the thermal conductivity.

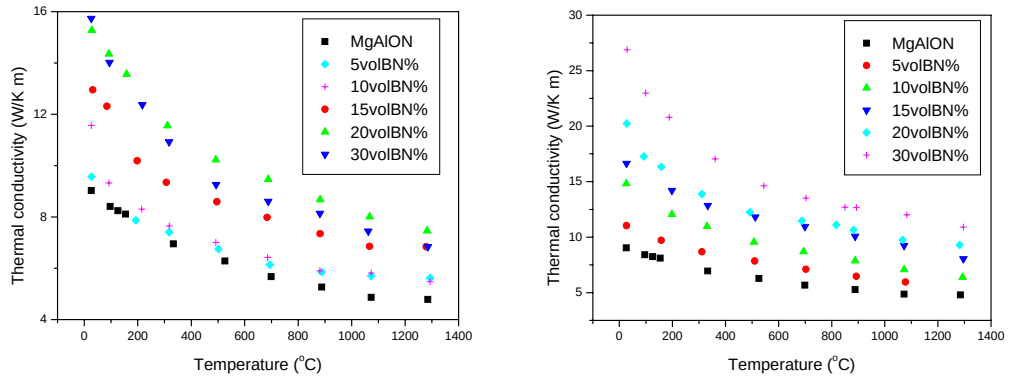

Figure 13. Temperature dependent of thermal conductivities of MgAlON and MgAlON-BN composites with different BN contents (a) parallel to hot-pressing directions. (b) perpendicular to hot-pressing directions.

4.5 Sessile drop experiment

The sessile drop experiments were carried out both in purified argon gas as well as in a given oxygen partial pressure.

4.5.1 Molten iron on MgAlON-BN composites

The contact angle measurements of pure iron were carried out on three different substrates, MgAlON, MgAlON-15vol%BN and MgAlON-30vol%BN respectively, using three different oxygen partial pressures at two different temperatures. The partial pressures of oxygen were controlled by mixing Ar-CO-CO_2 carefully. The calibration of the X-ray sessile drop technique was carried out by Kapilashrami et al[36] and Jakobsson et al[37] using Cu, Ni and Fe, which confirmed the reliability of this technique.

The results obtained for contact angle measurements under purified argon gas with different substrates showed that contact angles were almost constant in the temperature range 1823 to 1873 K, as can be seen from Figure 14. The points in the figure are the average values of numbers in two parallel experimental runs after 30 minutes stabilization. The results obtained in the present experiment have a value similar to those reported with alumina substrate earlier in the present laboratory[36]. On the other hand, the contact angles of MgAlON-BN composites were higher than those for Al_2O_3. The

error in the present experiment was estimated to be ±4º. The x-ray images of liquid iron drop on different substrates are presented in Figure 15.

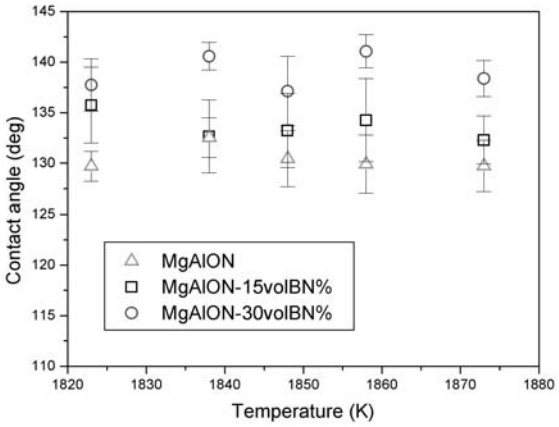

Figure 14. The contact angle between substrates and liquid iron at different temperatures.

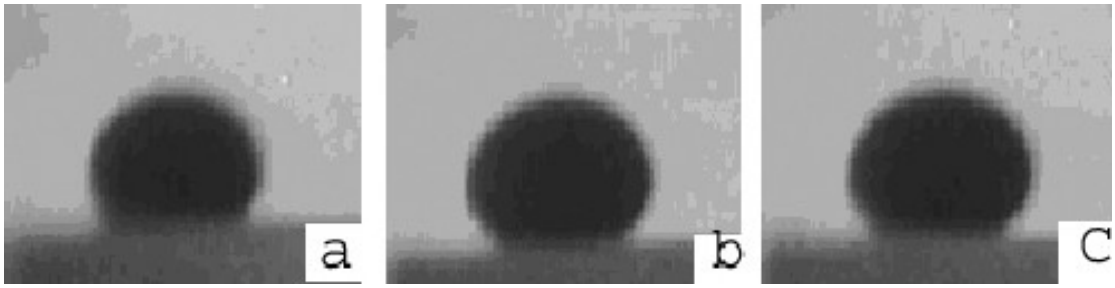

Figure 15. The images of liquid iron over substrates ((a) Pure MgAlON, (b) MgAlON-15vol%BN, (c) MgAlON-30vol%BN) in purified argon atmosphere after 30 minutes.

Figure 16 shows the variation of contact angles at various time intervals at 1823 K under oxygen partial pressures P_{O_2}=9.9×10^{-4} *Pa* and P_{O_2}=1.5×10^{-2} *Pa* respectively. The zero time marks the onset of the gas mixture, and the gas mixture may need approximately 120 seconds to reach the liquid iron drop. The contact angle in this time interval remained constant, as can be seen from Figure 16. After this, the contact angle showed a drastic drop and later a slow decrease, reaching a steady value at last.

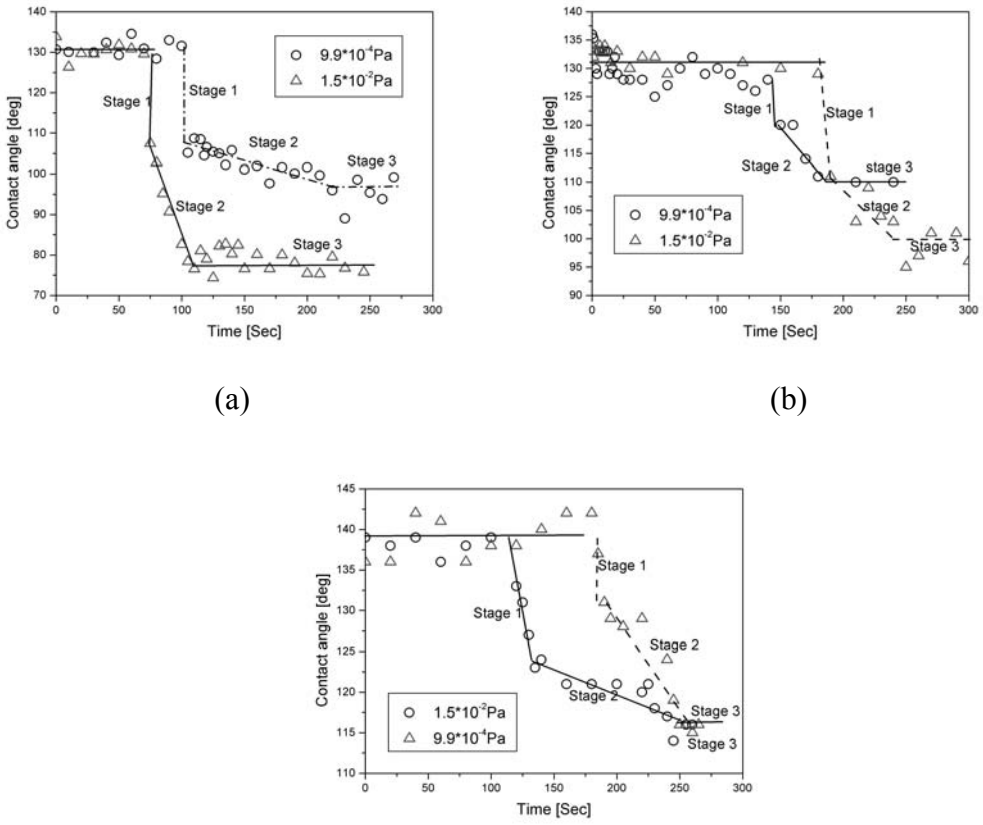

Figure 16. Contact angles variation between substrates and liquid iron at 1823 K as function of time under different oxygen partial pressures. a: pure MgAlON; b: MgAlON-15vol%BN; c: MgAlON-30vol%BN

4.5.2 Molten slag on MgAlON-BN composites

Gas bubble generation was observed during the experiments with the x-ray sessile drop unit. Figure 17 presents the X-ray images of slag on dense MgAlON at 1400 ^{o}C for various time intervals. As can be seen, active generation of gas bubbles was noticed and this continued during the experiment. The number of gas bubbles increased with increasing time, and the gas escape continued up to 20 min. There was then a brief pause of 10 min after which the gas bubbles formation continued again. Figure 18 gives the X-ray images of slag on dense MgAlON-15vol%BN composites at 1350 ^{o}C, which shows the same pattern with that in Figure 17. Gas bubbles generation was not observed when the temperature is lower than 1350^{o}C.

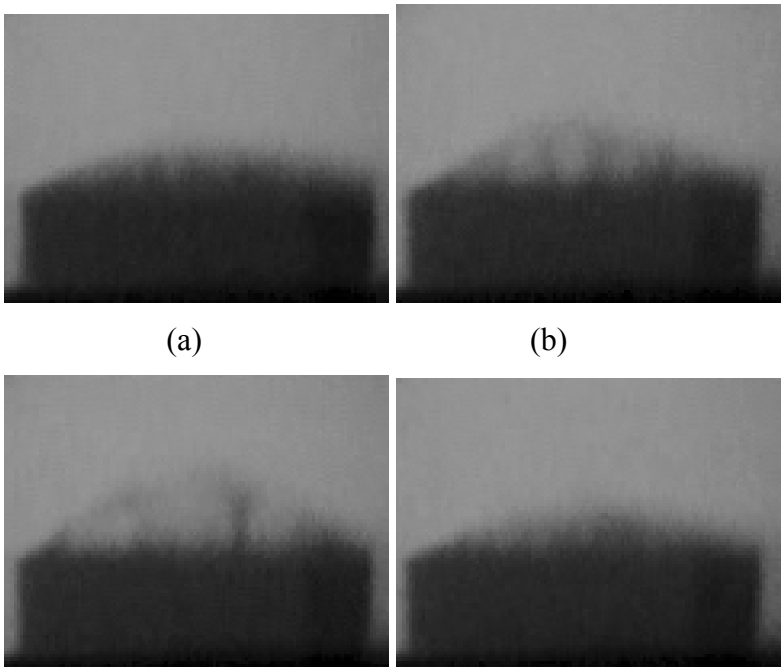

(a) (b)

(c) (d)

Figure 17. X-ray images of slag on MgAlON substrate at different time at T=1400^{o}C (a)0min, (b)10min, (c)20min and (d)30min

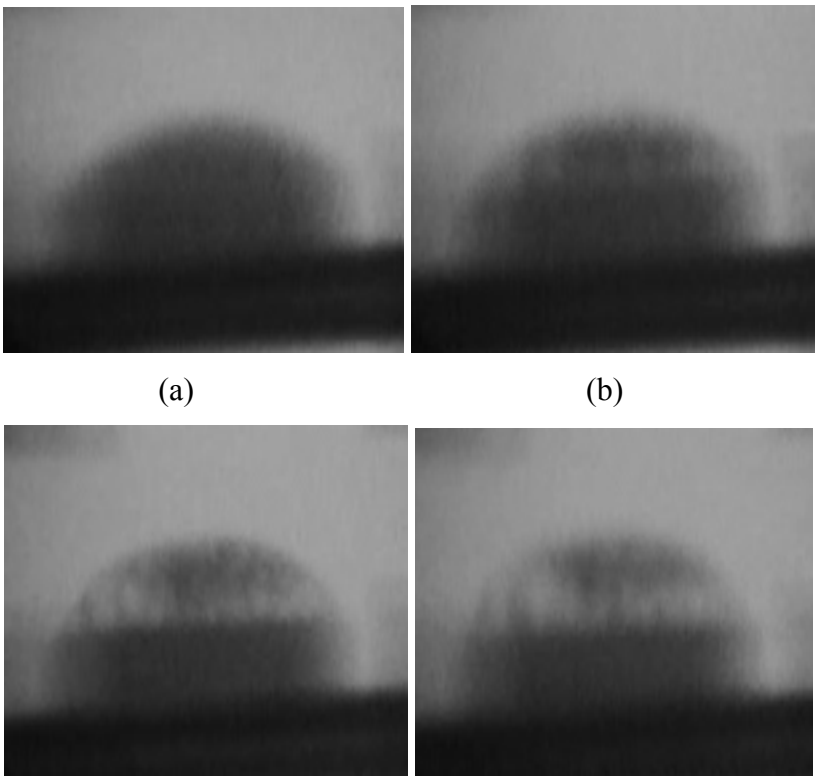

(a) (b)

(c) (d)

Figure 18. X-ray images of slag on MgAlON-15vol%BN substrate at different time at T=1350^{o}C (a)0min, (b)10min, (c)20min, (d)30min

4.6 Slag corrosion experiment

In the present paper, ΔR is defined as the radius difference between the initial radius of the cylindrical specimen and that after slag corrosion at a given time, and is used to denote the extent of corrosion of the sample. The change in rod radius as a function of square root of time for MgAlON-15volBN% composites at different temperatures corroded by slag No.1 is shown in Figure 19(a). It can be observed that a linear dependency exists for the MgAlON-15vol%BN composites. ΔR increased with increasing time and with increasing temperature. In the next series, a slag containing 10wt% FeO corresponding to slag No.2 was used in order to examine the effects of FeO addition on the slag corrosion rate. The experimental results are presented in Figure 19(b). It can be seen that FeO addition has a significant effect on the corrosion rate. To see the effect of BN addition on the corrosion rate, the slag corrosion resistance of the composites containing different BN contents were examined at 1390°C and 1420°C respectively. The experimental results indicated that ΔR decreased with increasing of BN contents.

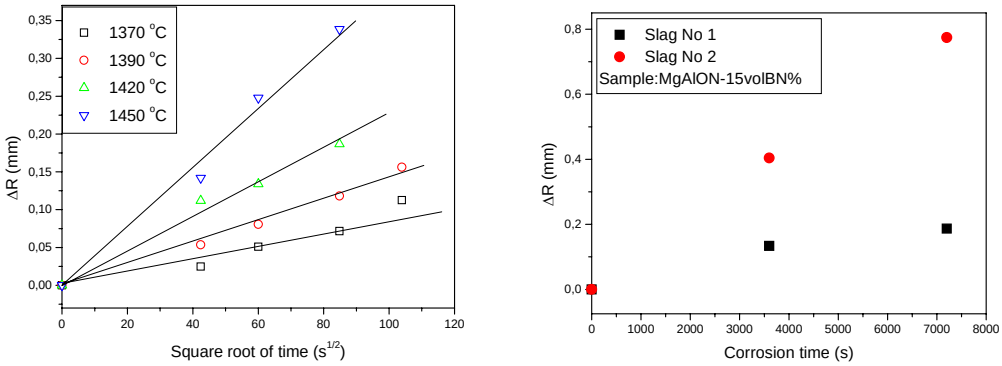

(a) (b)

Figure 19. Corrosion rate at different temperatures as a function of square root of time

5 Discussion

5.1 Microstructure evolution of MgAlON/BN composites

Figure 6 shows scanning electron micrographs of fracture surfaces of sintered composites without BN as well as with 10, 15 and 30vol% h-BN additions. These surfaces represent planes perpendicular to hot pressing direction. The fracture modes for MgAlON and composites containing 5vol%BN were found to be a mixed transcrystalline and intercrystalline, and for composites containing 15vol%BN and 30vol%BN, however, was

found to be a mixed intercrystalline and cleavage fracture. Equiaxed MgAlON grains, about 2~3 μm in size, were observed in monolithic MgAlON and MgAlON/h-BN composites containing different h-BN volume fraction. H-BN, about 200~300 nm in thickness as well as 1~3μm in length, grew in flake shape configuration, and it was evident that BN grains was preferentially oriented with the basal plane perpendicular to

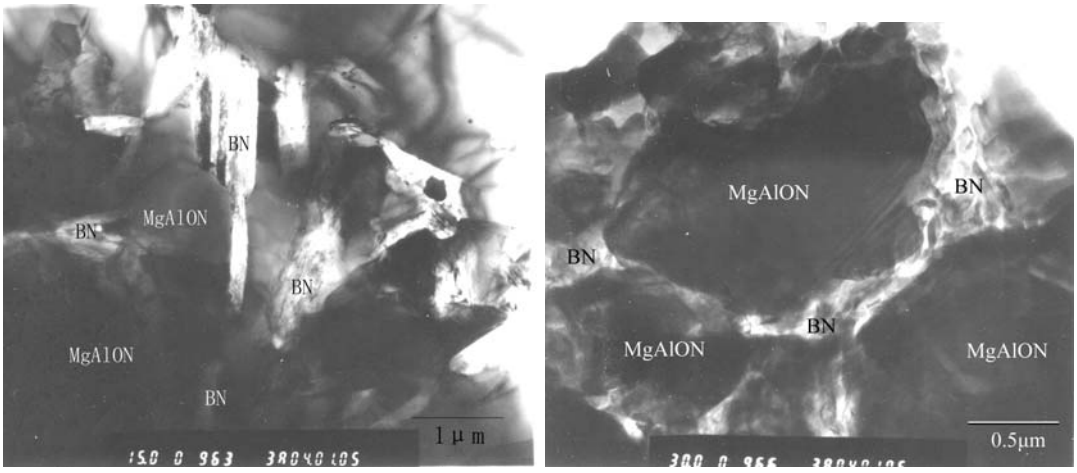

15vol% 30vol%

Figure 20. TEM photographs of the composites containing different BN contents

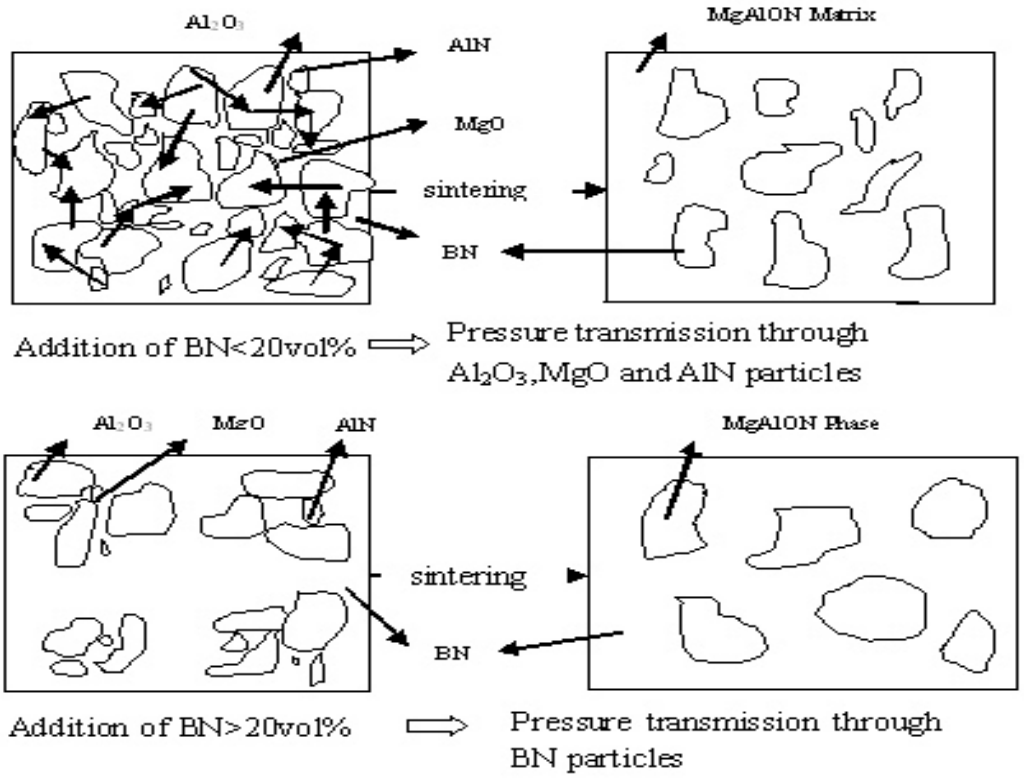

Figure 21. Pressurized sintering mechanism of MgAlON-based composite ceramic

the direction of hot-pressing, as can be seen from Figure 20. Experimental observations revealed that the hexagonal BN flakes were dispersed among MgAlON grain boundaries. The TEM results shown in Figure 20 indicated that the MgAlON phase was continuous in a composite when BN amount was 15vol%. However, addition of 30vol%BN made the microstructure to maintain a discontinuous network. In the process of synthesizing MgAlON-BN composites, it was considered that pressure was mainly transmitted through Al_2O_3, AlN and MgO powders when the BN content was lower than 20vol%. This resulted in a continuous microstructure with MgAlON. The pressure, however was amainly transmitted through BN powders when BN is more than 30vol%, which would lead to the discontinuous microstructure. Figure 21 gives a schematic of sintering mechanism.

5.2 The effect of BN addition on properties of the composites

H-BN exhibits considerable anisotropy of many of its properties such as thermal expansion, thermal conductivity as well as thermal diffusivity and demonstrates low Young's modulus, density properties and non-reactive nature. The presence of an inert BN phase in the MgAlON matrix which has limited sinterability decreases the densification rate of the composites. These resulted in the decrease of relative density, hardness, Young's modulus of composite ceramics with increasing of BN volume fraction, and consequently led to the decrease of bending strength.

The generation of microcracks: In cooling from the fabrication temperature, a particle with a larger thermal expansion coefficient than the matrix induces tangential compressive stresses and radial tensile stresses. Alternatively, particles with a smaller thermal expansion coefficient create tangential tensile stresses and radial compressive stresses[38]. For the present case, the thermal expansion coefficients of BN in different directions are $\alpha_{\perp}=1\times10^{-6}K^{-1}$ and $\alpha_{//}=7.51\times10^{-6}K^{-1}$, respectively. The thermal expansion coefficient of MgAlON is $\alpha=5.31\times10^{-6}K^{-1}$. At the MgAlON/BN interface parallel to the hexagonal axis of BN, the radial compressive stress may clamp the interface, forming some microcracks, whereas at MgAlON/BN interface perpendicular to the hexagonal axis of BN, the radial tensile stress may also form some microcracks, as can be seen from Figure 22. Thermal residual stresses induced by thermal expansion mismatch can be calculated using the Selsing equation[39].

$$P^{res} = \frac{2(\alpha_m - \alpha_p)\Delta T E_m}{(1+v_m)+2\beta(1-2v_p)} \tag{35}$$

where $E_m, E_p, v_m, v_p, \alpha_m$ and α_p are Young's modulus, Poisson's ratios and thermal expansion coefficients of the matrix and particle. ΔT is the temperature difference between fabrication temperature ignoring the plastic transform and room temperature. Thus, thermal stresses on the interfaces parallel and perpendicular to the hexagonal axis of BN were calculated, and the values were 364.6 MPa and -176.7MPa, respectively. The anisotropy of BN also can induce the thermal stresses, and these could be described as follows[20],

$$\sigma_z = \frac{E\Delta T}{(1-v^2)}\left[(\alpha_{//} - \alpha) - v(\alpha_{\perp} - \alpha)\right] \tag{36}$$

where E and α are the mean Young's modulus and thermal expansion coefficient of composite materials, respectively. These values can be calculated using composite law. Thus, the thermal stresses can be calculated by Eq.(36) and the value was -417.4MPa. It should be pointed out that overall residual stresses were not the sum of above three values. These can be explained by the following reasons: (1) BN particles are distributed on the grain boundaries of MgAlON. This increases the randomness of orientation of BN particles, and consequently changes the anisotropy of BN with respect to thermal expansion coefficient; (2) It is impossible to fabricate the full dense composites, the porosity in composites can absorb some elastic energy and consequently results in the decrease of the residual stresses; (3)The change of physical parameters with thermal shock temperature difference, such as Young's modulus, Poisson's ratio and thermal expansion coefficient are ignored. As can be seen from Figure 22, there are some mirocracks with several micrometers length in the composite materials induced by the thermal stress. It's far lower however than the calculated values shown in Table I. This indicates that the microcracks have small influence on the strength of composites, but may have much effect on other physicochemical properties, such as the bending strength at elevated temperature, fracture toughness, thermal shock durabiliiy and thermal conductivity etc.

Table I Parameters affecting thermal shock durability, ΔT_c for MgAlON, MgAlON-BN and BN ceramics

	MgAlON	-15vol%BN	-30vol%BN	h-BN
E(GPa)	207	182.65	110.01	65
$\gamma_{wof}(J\cdot m^{-2})$	535.95±11.81	412.20±23	334.80±15.37	---
$\alpha\ (K^{-1})$	5.31×10^{-6}	[a] 4.814×10^{-6}	[a] 4.275×10^{-6}	1.0×10^{-6}
v	0.25	[a] 0.24	[a] 0.24	0.23
σ *(MPa)*	379.68	294.4	168.59	28
K_{IC} $(MPa\cdot m^{-2})$	3.23	3.64	2.26	---
C(μm)	32	67	63	---

[a] Calculated using "Composite law" based on the values of each monolithic, MgAlON and BN

[o] Calculated using equ. $K_{IC} = (2E\gamma_i)^{1/2} = (\sigma YC^{1/2})$, where Y=1.5

E: Young's modulus, γ_{wof} work of fracture, α thermal expansion coefficient, v Possion's ratio, K_{IC} fracture toughness, C critical crack length.

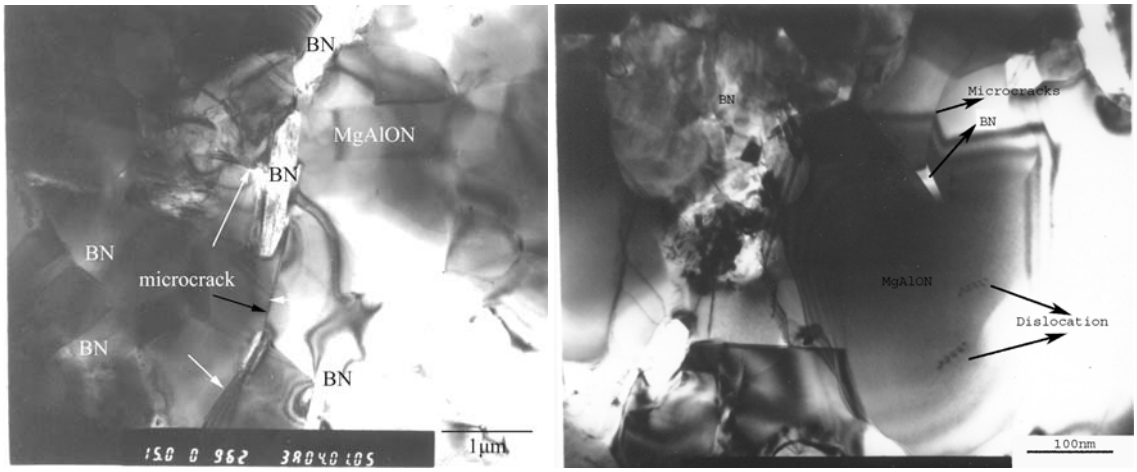

(a)crack deflection (b)grain boundary

Figure 22. TEM micrographs of (a)crack deflection and (b)grain boundary dislocation in sample with 15vol% h-BN

The influence of microcracks on mechanical properties: In the process of fracture of composites, as a propagating crack reaches a BN flake, the stresses acting on crack-tip will change from three dimensions to two dimensions because of the h-BN flakes. Hence, the crack-tip is blunted and deflected, and the deflection will consume much energy in this process, which is positive for the fracture toughness, but negative for room temperature bending strength. In addition, the pullout effect is contributing to the increase of work of fracture toughness. But the BN addition beyond 20vol% is resultant in the microstructure change, and the defects increase correspondingly due to the non-reactive nature of BN. Thus the microcracks are limited to increase the fracture toughness in this case, and consequently the fracture toughness decreases correspondingly. The composites expand considerably at elevated temperature, and the residual stress and microcracks decrease correspondingly. In addition, the interwoven microstructure of h-BN in the composites containing 15vol%BN prevents grain boundary slip and reduces the attenuation rate of high temperature strength. This is likely to result in the increase of the bending strength, reaching the maximum value at $800^{o}C$. The softening of non-crystalline at high temperature leads to the decrease of bending strength. Furthermore, the new microcracks may be generated due to the continuous expansion with temperature increasing, and consequently leads to the decrease of bending strength. The convenience of machining is presumably attributed to the cleavage of the layered structure h-BN dispersed in the matrix, which may confine the machining damage to a very small region under the tip of the tools through microcracking to absorb and disperse the force during the machining operations. Linking of the microcracks result in the ease of machining.

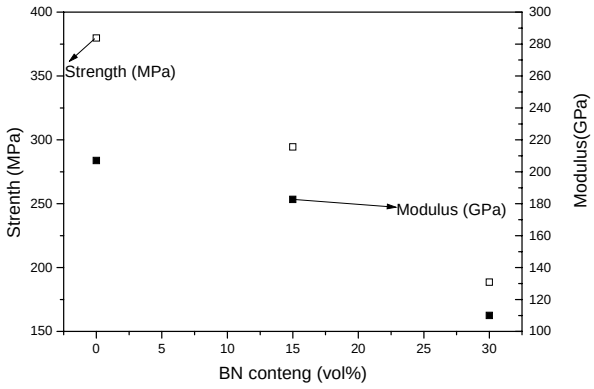

Figure 23. Strength and modulus as functions of BN contents

The influence of BN addition on thermal shock durability: The microcracks have the more negative effect on strength than Young's modulus with the 15vol% BN addition, as can be seen from Figure 23. This resulted in the slight decrease of R parameter. 30vol%BN addition however led to the discontinuous microstructure with MgAlON, as can be seen from Figure 20. BN flakes were distributed on the grain boundaries in this case instead of interwoven microstructure, and no obvious microcracks were found. On the other hand, the mean thermal expansion coefficient also decreased. This led to the increase of R parameter. Since the MgAlON-BN composite materials are not always resistant to fracture initiation by the thermal stress, the R''' and R'''' parameters must be taken into account in characterizing further thermal shock damage[25]. The R''' expresses the ability of a material to resist crack propagation and further damage and loss of strength on thermal shocking. The trends in the R''' parameter are consistent with the measurements of thermal shock damage caused by water quenching.

The sintering of the MgAlON-BN composite seems to be predominantly promoted by forming of MgAlON particles and the BN particles might prevent the contact between MgAlON particles and accordingly restrain the sintering of the composite. Thus, it can be concluded that the grain boundary energy between MgAlON grains is higher than that between MgAlON and BN grains due to the non-reactive nature of BN. This resulted in the decrease of work of fracture, and can be verified by the SEM analysis. The fracture surface of pure MgAlON showed part of intergranular cracks shown in Figure 6. Further addition of BN however lead to the occurrence of transgranular fracture. It appears that intergranular cracks require much more energy for fracture. Therefore, the lower values of γ_{WOF} are associated with the lower grain boundary energy and the occurrence of more intergranular fracture instead of transgranular fracture.

The influence on thermal conductivity: Boron nitride is always present as the hexagonal structure similar to that of graphite, which is an extremely good electrical insulator. Consequently, it has a fairly low thermal conductivity up to very high temperature in its hot-pressing form. Thus, it is a useful refractory material. No evidence of reaction or formation of solid solution between the MgAlON and BN was observed in the present experiment. At the same time, hexagonal-BN exhibits considerable anisotropy of its thermal conductivity/diffusivity, which results in the anisotropy for thermal diffusivity/conductivity of MgAlON-BN composites. The low Young's modulus, density properties and non-reactive nature would lead to the increase of the porosity and defect in

the composites. The thermal conductivity of BN along the c-axis($k_{//}$) is much smaller than that along the a-axis($k_{\perp}$). $k_{\perp}$ decreases with increasing of the randomness of orientation of BN particles. $k_{//}$, however, increases with increasing of the randomness. BN particles are preferentially oriented with basal plane perpendicular to the hot-pressing direction[14]. Since the thermal conductivity along the basal plane of BN is greater than that perpendicular to the basal plane, the effective thermal conductivity of MgAlON-BN composites should exhibit the similar trend, as can be seen from Figure 13. This behaviour has been demonstrated by the thermal diffusivity of hot-pressed composites of Si_3N_4-BN composites[40] and SiC-BN composite[41]. The degree of anisotropy for the composites has been defined as k(larger value)/k(smaller value)[42]. The degree of anisotropy values containing different BN contents was calculated and the value of degree of anisotropy was 1.15-1.71 at room temperature, and increased with increasing of the BN content. Generally, the degree of anisotropy decreases with decreasing size of BN[43]. BN particles distributed in composites are about hundreds nanometers in thickness as well as several micrometers in length, as can be seen from Figure 6 and 20. This results in the small degree of anisotropy. The thermal conductivity of a material is closely related to the microstructure of the materials. The phonons can strongly interact with point defects, line defects, planar defects, dislocations, grain and phase boundaries and finite size of the sample, which are included in the second term on the righthand side in Eq.(18). Therefore, the presence of BN phase, porosity, together with the nature of the interface of BN phase will have a significant influence on the thermal conductivity of the composites[44].

The effect on slag corrosion behaviour: The porosity of composites showed the increasing trend with increasing of BN content due to the non-active nature of BN. Thus, the pores in composites are likely to provide the channels for slag penetration. From this viewpoint, the slag resistance decreases with increasing BN. On the other hand, the BN addition leads to the change of microstructure. High resolution electron microscope (HREM) experimental results showes that there is no glass phase existing between the grain boundaries of MgAlON, and the grains of MgAlON are bonded directly. Some glass phase, however, is located at the triple junction nodes between MgAlON and BN grains. This leads to the decrease of the grain boundary interface energy greatly, and consequently increases the dihedral angle. In view of the fact that the porosity of composites caused by BN addition is limited, the slag corrosion resistance increases[12].

Furthermore, the contact angle between BN and molten slag or steel is higher than that with MgAlON, and consequently BN would not easily react with the components in slag. As the reaction proceeds, BN agglomerates at the interface between sample and product layer. The resistance to the diffusion of slag components towards the sample would correspondingly increase. Further, some B_2O_3 formed during the fabrication was likely to combine with some Al_2O_3 to yield $9Al_2O_3 \cdot 2B_2O_3$, which also increased the resistance of diffusion in product layer. These resulted in the increase of slag corrosion resistance.

It should be pointed out that BN particles would like to stick together easily to form agglomerates. One possible reason for the agglomeration of BN particles is that only a small amount of liquid is produced during the sintering process due to the low oxygen content in the starting powders. Thus, inhomogeneity of the formation and distribution of the liquid phase result in the presence of local regions of liquid in the microstructure and poor wetting in the neighboring regions. Therefore, the local liquid pools give high density regions surrounded by poorly sintered region, porosity and nano-sized grains. This microstructure must influence the mechanical properties of the material and porosity and consequently is detrimental to the strength and fracture toughness of the composite, and may act as fracture flaw, as can be seen from Figure 24. These phenomena has also been observed in TiN based composite ceramics[45].

Figure 24. Groups of nano-sized grains of BN agglomerates

From microstructural analysis, it can be seen that bending strength at room temperature and elevated temperature as well as fracture toughness of MgAlON/h-BN are closely related to its microstructure. Thus, in order to obtain a high performance MgAlON/h-BN

composites, some improvements are needed. First, a homogeneous microstructure is sought after which can be realized by controlling the starting powders. Secondly, a proper BN addition would be suitable in order to control the microstructure and the thermal mismatch between MgAlON matrix and h-BN flakes when the composite material is cooled to room temperature.

5.3 Modelling

The thermal conductivity of composites has been widely investigated theoretically over the past decades[48-53]. In most of these investigations, the inclusions in particulate composites were generally considered as being spherical[52]. Eucken[49,60] gave one equation to describe a minor amount of a discontinuous second phase dispersing uniformly in a continuous major phase. Figure 25 shows the comparison of the experimental data with the thermal conductivities calculated by Eucken's equation. It can

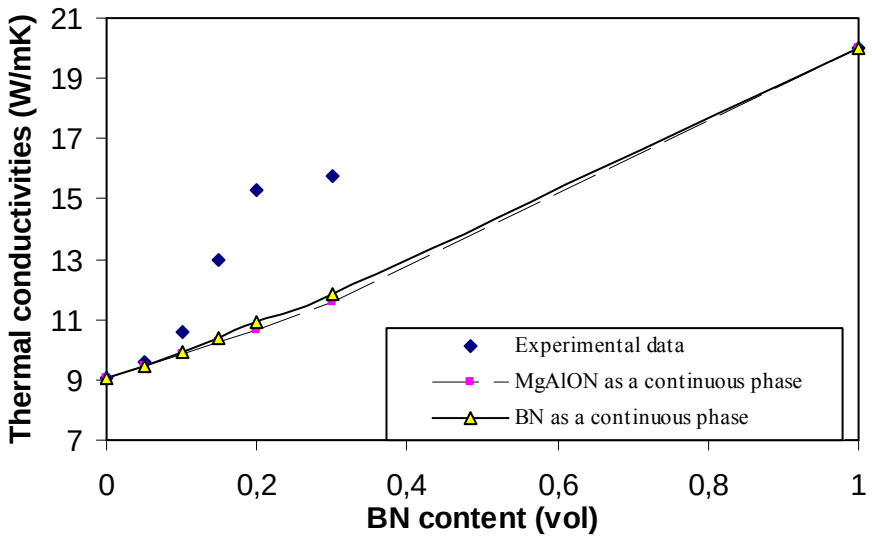

Figure 25. Relationship between BN content and the effective thermal conductivities of MgAlON/BN composites parallel to hot-pressing direction determined by Eucken's equation.

be seen that there is a large discrepancy between the experimental and calculated values especially when the BN addition is beyond 10vol%. This maybe due to the large amount of discontinuous second phase resulting in the defects or dislocation in composites, as can be seen Figure 22. Consequently, the composite ceramics always do not normally satisfy the isothermal interface condition[48]. Interfacial imperfections such as residual stresses, defects at the interface, and interfacial debonding caused by the mismatch of thermal

expansion coefficient or impurities reduce the thermal conductivity. These have been extensively confirmed for the case of ceramic-matrix composites[48, 54-56]. In composite ceramics, another important factor which can not be ignored is the effect of porosity on the thermal conductivity. Dunn[57] proposed a model to calculate the thermal conductivity of multiphase ellipsoid inclusion composites on the basis of Eshelby's model[53]. The pores in composite ceramics were evaluated by treating the porosity containing materials as a special case of the inclusion composites, with a zero thermal conductivity for the inclusions. Luo considered the special case, that of a particulate composite containing ellipsoidal pores and derived the equation which was suitable for SiC particle reinforced MgO composite ceramics[48]. It should be pointed out that the inclusions were distributed homogenously in composites in Luo's equation. However, in the present composites, BN was distributed on the grain boundaries of MgAlON, and part of them agglomerated, as can be seen from Figure 24. Therefore, we introduce one constant f(F) to describe the BN distribution in the composites. The equation based on Luo's equation can be described as follows,

$$\frac{f(F)}{K_{CP}} = \frac{K_M}{K_C K_P} + \frac{(K_M - K_P)(K_C - K_M)}{3K_M K_C K_P} \tag{37}$$

where F, K_C, K_M, K_P and K_{CP} are volume fraction of BN, the thermal conductivities of the fully dense composites, matrix, the matrix with some porosity, and composites containing pores, respectively. The constant f(F) is proportional to the volume of BN, and f(F)=0.961+0.019F for the composites parallel to hot-pressing direction, f(F)=1.023+0.0363F for the composites perpendicular to hot-pressing direction. K_C can be calculated by Eq.38, which took into account of the effect of interfacial thermal conditions[58].

$$K_C = \frac{2\lambda(1-F) + \beta[3 + (\lambda - 1)(1 + 2F)]}{\lambda(2 + F) + \beta[3 + (\lambda - 1)(1 - F)]} K_M \tag{38}$$

where the parameter β represents the interfacial thermal condition of the composites, and $\lambda = K_I / K_M$. F is the volume fraction of the inclusions. K_P in Eq. 37 can be expressed as,

$$K_P = \frac{1 - F_P}{1 + (\eta_2 - 1)F_P} K_M \tag{39}$$

where F_P is the volume fraction of the porosity and η_2 is a parameter which is related to the shape of porosity. The minimum value of η_2 is 2, for ellipsoidal pores[17,28]. In order to elucidate the applicability of this model to the present work, the parameter β

value was needed. β=3-10 were used by Luo and Stevens[17] to calculate the SiC particle reinforced MgO composites, which was also used in the present prediction. Figure 26 shows the comparison of the experimental data with the thermal conductivity calculated by Eq. 37. It can be seen that there is a small discrepancy between the experimental results and calculated values, especially the composites containing 30vol%BN. The discrepancy can be attributed to many factors as mentioned earlier. The addition of BN induced thermal stresses, dislocation, impurities and interfacial conditions.

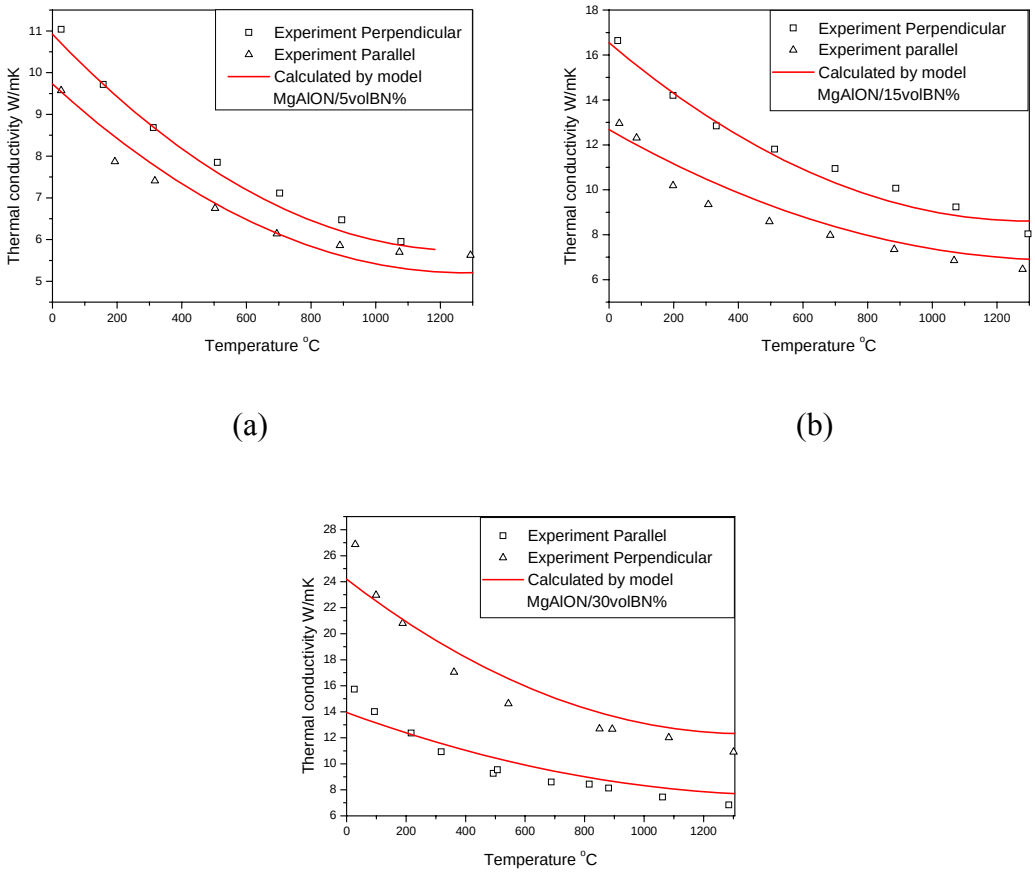

Figure 26. Comparison of the effective thermal conductivities of MgAlON/BN composites between the experimental results and predicted lines determined by present model. (a)5vol%BN composite (b) 15vol%BN composite and (c) 30vol%BN composite.

6 Summary and conclusion

MgAlON and MgAlON-BN composites were synthesized based on the phase stability diagram, and the mechanical properties, thermal shock durability, thermal diffusivity/ conductivity, wetting characteristics as well as slag corrosion mechanism were investigated systematically in the present project. The conclusions should involve:

(1) The Gibbs energy of MgAlON was calculated, and thermodynamic calculation of Mg-Al-O-N-B system was carried out in the present paper. MgAlON-BN composites were thus fabricated based on thermodynamic prediction. XRD was used to analyze MgAlON-BN composites. The experimental results indicate that the main phase is MgAlON, and the second phase is BN. No impurities are found.

(2) A matrix-flushing method for quantitative analysis of BN content in composites by X-ray diffraction was carried out. The results indicated that some AlN and MgO or Al_2O_3 evaporated during sintering process.

(3) SEM, TEM as well as HREM were used to characterize the microstructure of MgAlON/BN composites. The results indicate that the equiaxed grains are MgAlON, and the rod-like or flake-like grains are BN. BN particles are dispersed on the grain boundaries. There is no glass phase existing between the grain boundaries of MgAlON, and the grains of MgAlON were bonded directly. Some glass phase, however, is located at the triple junction nodes between MgAlON and BN grains.

(4) There was a significant decrease in the bending strength, Vickers hardness and density with increasing h-BN content due to the low density and poor densification behavior of h-BN. The enhancement of the fracture toughness was mainly attributed to the interwoven microstructure of h-BN and the microcracks induced by expansion coefficient mismatch between MgAlON and h-BN. The bending strength was found to increase with increasing temperature, and reaching the maximum value at $800^{o}C$, then decreased to 231 MPa at $1200^{o}C$.

(5) The thermal shock experimental results show that the strength of composite materials remains constant for a substantial temperature range followed by strength degradation gradually. The fraction of retained strength was improved from 37% to 53% at the thermal temperature difference 1500^{o}C. The experimental results showed the same trends with the calculation of R''' and R''''.

(6) The X-ray sessile drop experimental results show that the contact angles keep almost

constant under purified argon gas. Boron nitride was found to increase the contact angle from 132º for pure MgAlON to 135º and 139º for composites containing 15vol%BN and 30vol%BN. When the CO-CO_2-Ar gas mixtures were introduced into the system, it was found that Marangoni effect resulted in the movement of iron drop. The oxidation products combined with the FeO formed by oxidation of Fe to build a ternary or quaternary FeO-Al_2O_3-MgO(-B_2O_3) slag as shown by XRD analysis and SEM(EDS) analysis.

(7) Thermal diffusivity and heat capacity of MgAlON-BN composites were measured in the present work. The thermal diffusivity decreased rapidly with increasing temperature below 900^{o}C, while a slower decrease was observed with further increasing of temperature. This can be explained by the fact that the change of phonon mean free path gets a fixed value at very high temperature. Effective thermal conductivity exhibits the similar trend with thermal diffusivity. The addition of BN has a significant effect on the thermophysical properties of the composites. The anisotropy of BN results in the anisotropy of composites. The degree of anisotropy is small compared with that of BN. These maybe due to the agglomeration of BN at the grain boundaries.

(8) The rate of dissolution of dense MgAlON and MgAlON-BN composites in synthetic CaO-SiO_2-Al_2O_3-MgO-"FeO" slag has been investigated under stagnant conditions. The experimental results indicated that one product layer was formed during the slag process, and the product layer consisted of several reaction products. The radius difference between the initial and unreacted core showed a linear dependency exists for MgAlON-15volBN% composites with the square root of time. This indicated that the diffusion of ions in the slag through the product layer was the rate-determining step. The apparent activation energy of slag penetration between MgAlON-15vol%BN and slag No.1 was evaluated to be 376.4 kJ/mol. The gas bubbles were generated because of the reaction between slag and MgAlON. BN addition could improve the slag corrosion resistance. However, FeO addition into slag obviously increased the corrosion rate due to the oxidation properties to MgAlON/BN composites.

7 Future work

The work reported in this dissertation by the present author is part of an ongoing program at the present laboratory on the systemisation of different properties of refractories and its application in industry. In view of this, future work should involve:

(1) The presence of BN in MgAlON-BN composites provides many desirable properties such as excellent thermal shock and corrosion resistance. However, it is highly vulnerable to oxidation and induces low mechanical strength due to its weakly-bonded or non-active nature. In order to overcome these drawbacks, the antioxidants such as aluminium, silicon or Al/Mg alloys could be investigated during the fabrication process.

(2) The influence of antioxidant additives on the corrosion resistance and corroded microstructures of the composites should be investigated in the future.

(3) Investigation of MgAlON/BN composites using natural raw materials such as magnesite and bauxite or industry waste should be carried out in the future.

(4) In the future, the application of MgAlON-BN composites could be investigated in the real steelmaking process.

8 Reference

1. B. Narendra, P. Kadolkar and S. Swapnil: Surf. Interface Anal, 2001, vol.31, pp. 659–672

2. K.H. Jack, Review: J. Mater. Sci., 1976, vol. 11, pp.1135-1158

3. H. Hiroshi, Y. Akirs: J. Ceram. Soc. Jap., 2001, vol.109, pp.94-99

4. X.D.Wang, W.C. Li, S. Seetharaman: Z. Metallkde., 2002, vol.93, pp.540-544

5. X.D.Wang, W.C. Li, S. Seetharaman: Z. Metallkde., 2002, vol.93, pp.545-553

6. A. Granon, P. Goeuriot, F. Thevenot: J. Eur. Ceram. Soc., 1995, vol.15, pp.249-254

7. G.J. Zhang, J.F. Yang, A. Motohide, O. Tatsuki: J. Eur. Ceram. Soc., 2002, vol.22, pp.2551-2554

8. E.H. Lutz, M.V. Swain: J. Am. Ceram. Soc., 1992, vol.75(1), pp.67-70

9. S. Hayama, M. Ozawa, S. Suzuki: J. Ceram. Soc. Jpa., 1996, vol.104, pp.828-831

10. G.J. Zhang and Z.Z. Jin: J. Chin. Ceram. Soc., 1994, vol.22(3), pp.259-268

11. Z.D. Guan and Z.T Zhang: Physical properties of inorganic materials. Published by Tsinghua Univeristy, 1998.

12. W.E. Lee and S. Zhang: International Materials Review, 1999, vol, 44 No.3, pp.77-104

13. W.Y. Sun, L.T. Ma, D.S. Yan: Chinese Science Bulletin, 1990, vol.35, pp.200-202

14. H.X. Willems, R. Metsellar: Journal of European Ceramic Society, 1993, vol.12, pp.43-49

15. L. Kaufman: CALPHAD, 1979, vol.3, pp.275-291.

16. H.X. Willems, M.M.R.M. Hendrix, R. Metselaar, G. de With: J. Eur. Ceram. Soc., 1992, vol.10, pp.327-337.

17. L. Kaufman, H. Nesor: Metallurgical Transactions, 1974, vol.5, pp.1623-1629

18. L. Kaufman, H. Nesor: Metallurgical Transactions. 6A, 1975, vol.6, pp.2115-2121

19. L. Kaufman, H. Nesor: CALPHAD, 1978, vol.2, pp.35-53

20. L. Kaufman, H. Nesor: CALPHAD, 1979, vol.3, pp.27-44

21. L. Kaufman, H. Nesor: CALPHAD, 1981, vol.3, pp.163-184

22. B. Frank, H. Chung: J. Appl. Cryst, 1974, vol.7, pp.519-525

23. D.P.H. Hasselman: J. Am. Ceram. Soc., 1969, vol.52(11), pp.600–604.

24. D.P.H. Hasselman: J. Am. Ceram. Soc., 1963, vol. 46(11), pp.535–540.

25. A.Cemail, P. D.Warren: J. Eur. Ceram. Soc., 2003, vol.23, pp.301-308
26. A.Cemail, P. D.Warren, F.L.Riley: J. Eur. Ceram. Soc., 2004, vol.24, pp.2407-2416
27. G. Grimvall: Thermophysical Properties of Materials-Enlarged and revised edition. Elsevier Science B.V., Amsterdan, 1999, pp.254-285
28. M. Hayashi, A.A. Riad, S. Seetharaman: ISIJ International, 2004, vol.44(4), pp.691-697
29. H.X. Willems, G. de With and R. Metselaar: J. Eur. Ceram. Soc., 1993, vol12(1), pp.43-49
30. Standard test method for flexural strength of advanced ceramics at ambient temperature. In Annual Book of ASTM Standards, Designation: C1161-90, 15.01, 1991, pp.327-333.
31. K. Niihara, R. Morena and D.P.H. Hasselman: J. Mat. Sci. Letters, 1982, vol.1, pp.13-16
32. T. Sterneland, R.E. Aune and S. Seetharaman: K. Scandinavian J. Metall., 2003, vol.32, pp.233-240
33. Z.T. Zhang, T. Matsushita, W.C. Li and S. Seetharaman: Metall. Mater. Trans. B, 2006, vol.4. In press.
34. Xu, Hockin H.K. and Jahanmir, Said: J. Am. Ceram. Soc, 1995, vol.78(2), pp.497-500
35. El-Raghy T., S.Chakraborty and M.W. Barsoum: J. Eur. Ceram. Soc., 2000, vol.20, pp.2619
36. E. Kapilashrami, A. Jakobsson, A.K. Lahiri and S. Seetharaman: Metall.Mater. Trans. B, 2003, vol. 34B, pp.193-99
37. A. Jakobsson, N.N.Viswanathan, S.C. Du and S. Seetharaman: Metall. Mater. Trans. B, 2000, vol. 31B, pp.973-80
38. S. Jiao, M.L. Jenkins and R.W. Davidge: Acta mater. 1997, vol.45(1), pp.149-156.
39. J.Selsing. Internal stresses in ceramics. J. Am.Ceram. Soc., 1961, vol.44(8), pp.1419
40. K. Niihara, L.D. Bentsen, D.P.H. Hasselman, K.S. Mazdiyasni: J. Am. Ceram. Soc., 1981, vol.64(9), pp.C117-118
41. R. Rubert: J. Am. Ceram. Soc., 1984, vol.5, pp.C83-85
42. T.O. Kanai and K. Tanemoto: Jan. J. Appl. Phys., 1993, vol.32, pp.3544-3548
43. M.L. Dunn et al.: J. Compos. Mater., 1993, vol.27, pp.1473-519
44. J. Luo and R. Stevens: J. Am. Ceram. Soc., 1997, vol.80(3), pp.699-704
45. F.F. Xu, S.L. Wen, L.O. Norsberg and T. Ekstrom: Mater. Letters, 1998, vol.34, pp.248-252.

46.D.P.H. Hasselman: Am. Ceram. Soc. Bull. 49 12 (1970), pp. 1033–1037. 47.D.P.H. Hasselman: J. Am. Ceram. Soc., 1969, vol.52(8), pp.458–459.

47. Robert C. West, Ed. CRC Handbook of Chemistry and Physics, 60th Edition, CRC Press, Inc, Boca Raton, Florida, 1980, pp.B-94

48. J. Luo and R. Stevens: J. Am. Ceram. Soc., 1997, vol.80(3), pp.699-704

49. A. Eucken: Forsch. Geb. Ingenieurwes, 1932, vol. 353, pp.1-16

50. D.W. Richarson: Modern ceramic engineering. Second ed. New York: Marcel Dekker Inc; 1992. pp. 142-146

51.N. Nitani, T. Yamashita, T. Matsuda, S.-I. Kobayashi and T.Ohmichi: J. Nucl Mater, 1999, vol.274, pp.15-22

52. Y. Benveniste: J. Appl. Phys., 1987, vol.61, pp. 2840-43.

53. H. Hatta and M. Taya: Int. J. Eng.Sci., 1986, vol.24, pp.1159-72

54. A.J. Reeves, R.Taylor and T.W. Clyne: Mater. Sci. Eng. A, 1991, vol.141, pp.129-38.

55. L.M. Russell, L.F. Johnson, D.P.H. Hasselman and R.T.Ruh.: J. Am. Ceram. Soc., 1987, vol.70, pp.C-226-C-229.

56. S.P. Turner, R. Taylor, F.H. Gordon, and T.W. Clyne: J. Mater. Sci., 1993, vol.28, 3969-76.

57. M.L. Dunn et al.: J. Compos. Mater., 1993, vol.27, pp.1473-519.

58. D.P.H. Hasselman and L.F. Johnson: J. Compos. Mater., 1987, vol.21, pp.508-15

59. J. Luo and R. Stevens: J. appl. Phys., 1996, vol.79, pp.9057-63

60. K. Hayashi, T.M. Kyaw and Y. Okamoto: High Temp.-High Press., 1998, vol.30, pp.283-290